PORE NETWORK CONNECTIVITY AND ITS IMPACTS ON ELECTRICAL RESISTIVITY OF ANISOTROPIC ROCKS WITH COMPLEX PORE STRUCTURE

A Thesis

by

ABDELRAHMAN MOSTAFA KOTB

Submitted to the Office of Graduate and Professional Studies of
Texas A&M University
in partial fulfillment of the requirements for the degree of

MASTER OF SCIENCE

Chair of Committee, Zoya Heidari
Committee Members, Walter B. Ayers
Yuefeng Sun
Head of Department, Daniel Hill

December 2015

Major Subject: Petroleum Engineering

ABSTRACT

Core data and well-log interpretation results are usually comparable in homogenous conventional reservoirs. However, in the case of thinly-bedded, heterogeneous formations consisting of organic-rich mudrocks and carbonates, core-log calibration and integration are challenging. The calibration of well-log interpretation results with core data is hence justified for thick homogeneous beds. Consequently, petrophysical properties (e.g., fluid saturation) estimated from well logs are not generally in agreement with core measurements. Therefore, upscaling of petrophysical properties from core-scale to log-scale is essential to reconcile measurements obtained from different scales. Although petrophysical measurements vary from core-scale to log-scale, previous publications have shown that the relationship between formation factor and porosity is consistent over a wide-scale range in homogenous sandstones. These correlations, however, do not persist in rocks with complex pore structure and rock fabric (e.g., carbonates).

This research investigated the persistence of a correlation between the electrical resistivity and the directional connectivity tensor at different scales within the micron scale in sandstone and carbonate examples. To fulfill this objective, three-dimensional (3D), pore-scale rock images were obtained from micro-CT (Computed Tomography) images. Then, each 3D pore-scale image was divided into subsamples of varying sizes. Afterwards, tortuosity of the networks of the electrically conductive rock components (e.g., formation water) was estimated in each subsample. The next step was to numerically solve the Laplace's equation to estimate electric field distribution and effective electrical resistivity of each subsample. The last step involved calculating the directional connectivity tensor

based on the estimated tortuosity and volumetric concentration of each conductive component in the samples and subsamples. Finally, the impact of directional connectivity of pore network on electrical resistivity was quantified.

The results confirmed the existence of a correlation between directional connectivity and electrical resistivity at different micron scales in the samples studied in this thesis. Improvements of up to 59% and 54% were observed in the proposed relationship compared to the conventional relationship between porosity and electrical resistivity in fully and partially water-saturated samples, respectively. An improvement of up to 50% in estimates of water saturation was observed when the directional connectivity of pore network was taken into account.

DEDICATION

This thesis is dedicated to my supporting, cheering and loving parents, siblings, and wife.

ACKNOWLEDGEMENTS

In the name of ALLAH, the Beneficent, the Merciful.

I would like to express my gratitude to my creator, ALLAH SWT, for giving me strength, knowledge, and guidance to complete this master's thesis. All praise is for Him, who gives mankind the knowledge they never had before.

I would like to thank my advisor, Dr. Zoya Heidari, for her support, guidance, and valuable remarks and engagement through the conduct of this thesis. I also appreciate the help and support from the members of my committee, Dr. Walter B. Ayers and Dr. Yuefeng Sun for suggestions, guidance, assistance and patience from time to time during the process of this research.

I would like to thank all my colleagues in the Multi-Scale Formation Evaluation Research Group, especially, Artur Posenato, Emmanuel Oyewole, Gama Firdaus, Huangye Chen, Lu Chi, and Yuhai Zhou for their help and support in the completion of this thesis. I would like to thank the Texas A&M University Joint Industry Research Program for funding this work, jointly sponsored by Aramco Services Company, BHP Billiton, BP, Chevron, ConocoPhillips, and Devon Energy. I also want to thank the Department of Earth Science and Engineering in Imperial College London for providing micro-CT images in their open library. A note of gratitude goes to the W. D. Von Gonten Laboratories for making their facilities available for acquiring the micro-CT scans of core samples. I am also grateful for Don Conlee and John Maldonado at Texas A&M University for assisting me in acquiring the micro-CT scans and helping me cut the samples. I am also thankful to the

Texas A&M supercomputing facility for providing computing resources to conduct numerical simulations. Additional thanks goes to the Harold Vance Department of Petroleum Engineering staff and administration for being extremely helpful during my time in the department.

Last but not least, my sincere thanks and gratitude is to my mother, father, siblings and wife for their warm love, endless support, and help throughout the entire process.

TABLE OF CONTENTS

Page

LIST OF FIGURES

Page

LIST OF TABLES

Page

1. INTRODUCTION AND LITERATURE REVIEW

Interpretation of data from different scales (i.e., core-scale and log-scale) does not provide comparable results in complex carbonates due to the heterogeneity and anisotropy present in the formation. Using numerical simulation, this research achieved its objective to quantitatively identify a relationship between the directional connectivity tensor and the formation factor that persists at different scales in heterogeneous and anisotropic formations. The proposed relationship can be used in assessment of water saturation. This section elaborates on the background of this topic and presents its outline, statement of the problem, and research objectives.

1.1 Literature Review

The literature review is organized into four main sections. The first section presents the work done on the impact of rock structure on the electrical resistivity. The second section describes previous literature written discussing tortuosity in complex formations (e.g., carbonate formations) and how tortuosity is related to directional connectivity. The third section covers different methods used to estimate water saturation. The final section covers how the rock physical properties vary from reservoir-scale to pore-scale and previous work done to relate the different petrophysical properties at different scales. This subsection presents a comprehensive literature review to establish the current status of the work done related to this thesis's objectives.

1.1.1 Impact of the Rock Structure on Electrical Resistivity

Electrical conductivity of the rock is affected by the type of fluid present in the rock, the respective saturation, and the minerals forming the rock (Karato and Wang 2012). Measured electrical resistivity from well logs and lab measurements are used to examine the lithology and specify fluid saturations, which helps to estimate reserves and predict production performance (Schlumberger 1972, 1974; Doveton 1994). Fluid saturation in the log-scale is estimated using resistivity-porosity-saturation models (e.g., Archie's model (Archie 1942)). However, interpretation of electrical resistivity in complex and anisotropic formations is challenging (Man and Jing 1999). As a result of diagenesis in sedimentary rocks (i.e., compaction, dissolution, and cementation), the rock structure (i.e., pore and grain structure) in carbonate formations is complex (Moore 2001).

Experimentally investigating the effect of pore structure on the rock electrical behavior has been challenging due to the large number of variables affecting such behavior (Suman and Knight 1997). As a result, some theoretical studies have shown that pore structure significantly affects estimation of electrical resistivity of the rock (Chatzis and Dullien 1985; Wardlaw et al. 1987; Tsakiroglou and Payatakes 1991). Furthermore, other studies have shown that wettability also affects the resistivity of the rock. The saturation exponent in Archie's model was found to be higher in oil-wet systems than water-wet systems (Mungan and Moore 1968; Keller 1953; Sweeney and Jennings 1960; Rust 1957; Morgan and Pirson 1964; Lewis 1988; Donaldson and Bizerra 1985; Donaldson and Siddiqui 1989). Several studies have also experimentally concluded that for oil-wet rocks, the 'non-Archie' behavior can be observed (Swanson 1985; Diederix 1982; Worthington and Pallatt

1992; Worthington et al. 1989; Moss et al. 1999; Jing et al. 1990). Electrical resistivity of the rock is also affected by the stress applied to it (Brace and Orange 1966; Brace et al. 1965).

Previous research endeavors studied the influence of complexity and anisotropy on electrical resistivity measurements (Garing et al. 2014; Verwer et al. 2011). Garing et al. (2014) showed that pore network complexity in carbonate formations influences the electrical resistivity. The pore network complexity in carbonate formations impacts the relationship between electrical resistivity and porosity, which leads to uncertainty in fluid saturation estimation when conventional models (e.g., Archie's model (Archie 1942)) are used (Garing et al. 2014). Verwer et al. (2011) indicated that besides porosity, electrical resistivity is also affected by the pore structure. Reduced number of pores and poor connections impede the electric current flow (Verwer et al. 2011).

Besides electrical resistivity, the rock structure affects other properties such as tortuosity. The next subsection presents the relevant previous research performed on tortuosity of pore network and how it relates to electrical resistivity.

1.1.2 Tortuosity of Porous Media

Carman (1937) introduced tortuosity and defined it as the ratio of the effective path of flow to the length of the sample, given by

$$\tau = \frac{l_e}{l}, \tag{1}$$

where τ is the dimensionless tortuosity, l_e is the effective path, and l is the length of the sample. Although tortuosity is widely studied in many research fields besides petroleum (e.g., human brain and blood vessels) (Azegrouz et al. 2006; Hrabe et al. 2004), the understanding of tortuosity is still limited (Brakel and Heertjes 1974; Clennell 1997; Cornell and Katz 1953; Garrouch et al. 2001; Katsube 2010).

Tortuosity has been stated as a scalar property in some experimental work (Wyllie and Spangler 1952; Winsauer et al. 1952; Faris et al. 1954; Pirson 1983; Kastube 2010), where it is a function of porosity. However, there is evidence that tortuosity is dependent on permeability (Dullien 1975; Witt and Brauns 1983; Scheidegger 1954; Rice et al. 1970; Salem and Chilingarian 2000; Chapuis and Gill 1989), geodesic reconstruction of pore network (Selomulya et al. 2006), and diffusion process (Kim et al. 1987; Greenkorn and Kessler 1970; Ohkubo 2008; Whitaker 1999).

Clennell (1997) discussed four types of tortuosity, including geometrical, hydraulic, diffusional, and electrical tortuosity. Geometrical tortuosity (τ_g) is defined as the ratio of the shortest path connecting points in the fluid medium to the length of the sample. Hydraulic tortuosity (τ_h) is defined as the ratio of the shortest path a fluid takes from one point to another to the horizontal distance between the two points. Diffusional tortuosity (τ_d), introduced by Satterfiled and Sherwood (1963) and further studied by Greenkorn (1983) and Gao et al. (2014), is the ratio between the effective and bulk diffusivity. Finally,

electrical tortuosity (τ_e) is the ratio of the effective path of electric current to the length of the sample.

Although tortuosity affects electrical properties of the rocks and their interpretation for assessment of water saturation, there is no common agreement on how to measure or calculate tortuosity (Wyllie and Spangler 1952; Winsauer et al. 1952; Faris et al. 1954 Pirson 1983; Katsube 2010; Cornel and Katz 1953). The models proposed in previous publications calculate tortuosity as a function of formation factor and porosity. **Table 1** summarizes some of the models introduced to estimate tortuosity.

Table 1: Models Proposed to Estimate Tortuosity of Rock

Reference	Equation
Wyllie and Spangler (1952)	$\tau = (FF\phi)^2$
Winsauer et al. (1952)	$\tau^2 = (FF\phi)^{1.2}$
Faris et al. (1954)	$\tau^2 = (FF\phi)^{1.41}$
Pirson (1983)	$\tau = (FF\phi)^{0.5}$
Kastube (2010)	$\tau = (\frac{FF\phi}{b_f})^{0.5}$
Cornell and Katz (1953)	$\tau = FF\phi$
Bear (1972); Dullien (1979); Mota et al. (2001); Dias et al. (2006)	$\tau = \phi^{-p}$
Comiti and Renaud (1989); Mauret and Renaud (1997)	$\tau = 1 - p\,ln(\phi)$
Weissberg (1963); Iversen and Jorgensen (1993); Boudreau and Meysman (2006)	$\tau = 1 + p(1-\phi)$
Duda et al. (2011)	$\tau = 1 + p\sqrt{1-\phi}$

In equations included in **Table 1**, τ is the tortuosity, *FF* is the formation factor which is the ratio of total electrical resistivity of the sample to electrical resistivity of the formation water, ϕ is porosity, and b_f and p are constants that are functions of the shape of the connected pores.

Direct and indirect methods have been developed to estimate tortuosity in porous media. These methods include electrical resistivity (Barrande et al. 2007; Mast and Potter 1963), hydraulic conductivity (Comiti and Renaud 1989; Witt and Brauns 1983; Salem and Chilingarian 2000), and gas tracer tests (Kreamer et al. 1988). Three-dimensional (3D) images from X-ray microtomography can also be used to estimate tortuosity based on geodesic reconstruction (Gommes et al. 2009; Selomulya et al. 2006; Al-Omari and Masad 2004; Khan et al. 2012; Gao et al. 2012).

There exist other previous publications which correlated tortuosity to permeability (Dullien 1975; Bear and Bachmat 1990; Ghassemi and Park 2010). Furthermore, previous work introduced numerical techniques to estimate tortuosity of the pore network using pore-scale images (Nakashima et al. 2004; Nakashima and Kamiya 2007). Tortuosity has been estimated using nuclear magnetic resonance (NMR) as well (Latour et al. 1993; Latour et al. 1995; Sen 2004; Armatas 2006). Latour et al. (1993) succeeded in measuring tortuosity in a synthetic sample using NMR pulsed field gradient diffusion measurements. Latour et al. (1995) performed additional work to determine tortuosity using NMR pulsed field gradient technique (PFG). The equation proposed to calculate tortuosity is given by

$$\tau = \frac{1}{\frac{D(t)}{D_0} - \frac{\beta_1}{t} + \frac{\beta_2}{t^{3/2}}}, \quad (2)$$

where $D(t)$ is the diffusion coefficient, D_o is the fluid steady-state diffusion coefficient in the porous medium, t is the observation time, and β_1 and β_2 are constants that vary with microgeometry.

As mentioned earlier in this subsection, tortuosity serves as an input for some conventional resistivity-porosity-saturation models that are used to estimate water saturation. The next subsection covers previous literature that discusses the different models used in water saturation estimation.

1.1.3 Water Saturation Estimation

Water saturation is used to estimate hydrocarbon in place and reserves. Biases in estimates of reserves and hydrocarbon in place can occur when water saturation estimation is in error (Bowers and Fitz 2000; Hamada 2008; Widarsono 2012). Several models can be applied to estimate water saturation, and previous work has shown that significant difference in water saturation estimates can be observed from using different models (Worthington 1985; Widarsono 2012). **Table 2** contains some of the models used to estimate water saturation.

Table 2: Water Saturation Estimation Models

Reference	Equation
Archie (1942)	$S_w = \sqrt[n]{\frac{R_o}{R_t}}$
Hossin (1960)	$\sigma_t = \frac{\sigma_w}{FF} S_w^n + V_{sh}^2 \sigma_{sh}$
Simandoux (1963)	$\sigma_t = \frac{\sigma_w}{FF} S_w^n + V_{sh} \sigma_{sh}$
Bardon & Pied (1969)	$\sigma_t = \frac{\sigma_w}{FF} S_w^n + V_{sh} \sigma_{sh} S_w$
Poupon and Leveaux (1971)	$\sqrt{\sigma_t} = \sqrt{\frac{\sigma_w}{FF}} S_w^{n/2} + V_{sh}^{1-\frac{V_{sh}}{2}} \sqrt{\sigma_{sh} S_w^n}$
De Witte (1957)	$\sigma_t = \frac{\sigma_w}{FF} S_w^2 + A S_w$
Waxman & Smits (1968)	$\sigma_t = \frac{\sigma_w}{FF^*} S_w^n + \frac{B Q_v}{FF^*} S_w^{n-1}$
Dual water model: Clavier et al. (1984)	$\sigma_t = \frac{\sigma_w}{FF_o} S_w^n + \frac{(\sigma_{bw} - \sigma_w) v_Q Q_v}{FF_o} S_w^{n-1}$
Poupon et al. (1954)	$\sigma_t = V_{sh} \sigma_{Sh} + \frac{(1 - V_{sh}) \sigma_w S_w^2}{FF}$
De Witte (1955)	$\sigma_t = \frac{2.15 km_w}{FF} S_w^2 + \frac{km_{sh}}{FF} \sigma_w$
Patchett & Rausch (1967)	$\sigma_t = \frac{\sigma_w}{FF} S_w^2 + \sigma_s S_w$
Schlumberger (1972)	$\sigma_t = \frac{\sigma_w}{FF(1 - V_{sh})} S_w^2 + V_{sh} \sigma_{sh} S_w$
Juhasz (1981)	$\sigma_t = \frac{\sigma_w}{FF} S_w^2 + (\sigma_{sh} \phi^m - \sigma_w) \frac{V_{sh} \phi_{sh} S_w}{\phi}$
Alger et al. (1963)	$\sigma_t = \frac{\sigma_w (1-q)^2 S_w^2}{FF} + \frac{q(1-q))(\sigma_{sh} + \sigma_w)}{FF} S_w + \frac{q^2 \sigma_{sh}}{FF}$

Table 2: Continued

Reference	Equation
Husten & Anton (1981)	$\sigma_t = \frac{\sigma_w S_w^2}{FF} + 2V_{sh}\sqrt{\frac{\sigma_w \sigma_{sh}}{FF}}(1-\sqrt{\frac{\sigma_w}{\sigma_{bw}}})S_w + V_{sh}^2\sigma_{sh}(1-\sqrt{\frac{\sigma_w}{\sigma_{bw}}})^2$
Winsauer et al. (modified Archie's model) (1952)	$S_w = \sqrt[n]{\frac{aR_w}{\phi^m R_t}}$
Patchett & Herrick (1982)	$\sigma_t = \frac{(1-V_{sh})\sigma_w}{FF} S_w^2 + \frac{(1-V_{sh})}{FF} BQ_v S_w + V_{sh}\sigma_{sh}$
Woodhouse (1976)	$\sigma_t = \frac{\sigma_w}{FF} S_w^2 + 2\sqrt{\frac{\sigma_w V_{sh}^{2-2V_{sh}} \sigma_{sh}}{FF}} S_w^2 + V_{sh}^{2-2V_{sh}} \sigma_{sh} S_w^2$

In equations included in **Table 2**, S_w is the water saturation, R_o is the resistivity of the sample when the water saturation is 100%, n is the saturation exponent, R_t is the true sample resistivity, σ_t, σ_w, and σ_{sh} are the conductivities of the whole sample, water, and shale respectively, FF is the formation factor, V_{sh} is the volumetric concentration of shale in the sample, A is the shaliness factor, Qv is the cation exchange capacity per unit pore volume, B is the equivalent conductance of sodium clay exchange cations, FF^* is the intrinsic formation factor for a shaly sand, v_q is the amount of clay water associated with 1 unit of clay counterions, m_w and m_{sh} are the momal concentration of exchangeable cations in formation water and shale respectively, k is the conversion of m_w and m_{sh} to conductivity, m is the cementation factor, ϕ is porosity, a is tortuosity, and q is the fraction of total porosity occupied by clays.

All the equations mentioned in **Table 2** have an empirical origin. Worthington (1985) further categorized these water saturation equations. The first category includes the water saturation equations that take into account the volumetric concentration of shale. The second category includes the water saturation equations that take into account the volumetric concentration of shale as well as the double-layer models. The third category contains the equations that do not take into account the volumetric concentration of shale. Other work introduced some probabilistic solutions to estimate water saturation by using Monte Carlo simulation (Bowers and Fitz 2000). However, there is no agreement on one way to accurately estimate water saturation.

The previous subsections have discussed literature dealing with different physical and petrophysical properties of carbonate and sandstone formations (i.e., electrical resistivity, tortuosity, and water saturation). The upcoming subsection discusses how physical properties can be obtained from measurements at different scales. It further discusses models that correlate physical and petrophysical properties at different scales. Finally, it presents problems that occur from applying data from the pore-scale to the log-scale.

1.1.4 Rock Properties from Reservoir-Scale to Pore-Scale

The role of petrophysical properties is essential to a better understanding of the reservoir. Petrophysical properties (e.g., porosity, water saturation, and permeability) provide valuable information which can be used to select zones of completion. Estimation of petrophysical properties occur at different scales such as the reservoir scale where information is gathered from separate sources such as seismic measurements, gravity

surveys, and magnetic surveys. At the log-scale, data are gathered using well logs (e.g., gamma ray, resistivity, density, and neutron-porosity logs). At the core-scale, core-scale measurements (e.g., core flood) are conducted to estimate petrophysical properties (e.g., permeability). Finally, petrophysical properties can be estimated at the micro- or nano-scale using images obtained by scanning computed tomography (CT) and scanning electron microscope (SEM).

Some models correlate physical properties (e.g., electrical resistivity) to petrophysical properties (e.g., porosity) at different scales. However, these models can only be applied in homogenous formations. For instance, in the reservoir scale, previous publications investigated the scale-dependent acoustic wave propagation in heterogeneous formations (Mukerji and Mavko 1994; Yin et al. 1994). These studies investigated how the P-wave and S-wave vary at different scales of measurement relative to the reservoir scale. The results showed a significant variation of P-wave velocity and S-wave velocity at different reservoir scales in heterogeneous formations. At smaller scales (i.e., log-scale and pore-scale), other researchers assumed that core measurements are representative of the entire formation (Teh et al. 2011). Cinar et al. (2012) showed that the correlation between formation factor and porosity persists in conventional and homogenous formations. However, in heterogeneous formations, log-scale correlations between physical and petrophysical properties, such as electrical resistivity and porosity, are weak (Cinar et al. 2012; Teh et al. 2011). These weak correlations lead to unreliable assessment of petrophysical properties such as fluid saturation.

Still, other work applies core-scale data to the log-scale for rock typing (Pittman 1992). However, Xu (2013) mentioned four problems that occur when core-scale data are extrapolated to the log-scale. These problems are indirect measurements, poor data quality, scale discrepancy, and variable reservoir conditions. In the log-scale, petrophysical properties are not directly measured; rather the petrophysical properties are estimated using log-scale physical measurements (e.g., resistivity log and density log). Serra and Abbott (1980) categorized well logs depending on their sensitivity to the rock properties (i.e., composition, texture, structure and fluid). As an example, the nuclear magnetic resonance (NMR) log is most sensitive to the texture of the rock. On the other hand, other logs show high sensitivity to the composition of the rock (e.g., gamma ray log, photoelectric log, and acoustic log). Moreover, the structure of the rock influences the electrical resistivity logs. Finally, fluid saturation of the rock affects other types of logs (e.g., neutron porosity log, bulk density log, electrical resistivity log, acoustic log, and NMR).

Furthermore, the downhole environment and the complications that occur during operation affect well-log data quality. Theys (1999) explained some of these problems, including depth shift, mud filtrate invasion, and borehole rugosity. Deep mud filtration sometimes changes the fluid saturation near the borehole which results in inaccurate data acquired from the well logs (Salazar, 2004; Gandhi et al. 2010). Regarding scale discrepancy, measurements in well logs are conducted in the foot-scale resolution, whereas core data measurements are conducted in the inch-scale (Diniz and Torres 2012). Another scale-discrepancy problem results from different volumes of investigations

between well logging tools, which leads to increased uncertainty in estimating petrophysical properties in laminated and thinly bedded formations (Diniz and Torres 2012). Xu (2013) explained that reservoir properties (e.g., temperature, pressure, fluid saturations, and capillary pressure) change within the reservoir column. These changes in reservoir properties results in inconsistent log measurements of the same zones.

Overall, this literature review shows that previous studies found consistent relationships between physical properties (e.g., electrical resistivity) and petrophysical properties (e.g., porosity) at different scales (i.e., reservoir-scale and pore-scale) only in homogenous and isotropic formations. Furthermore, researchers do not agree on the definition of tortuosity, let alone a method to estimate either tortuosity or water saturation. In response to this problem, this thesis carries out numerical simulations to find a persistent correlation between physical and petrophysical properties at the pore-scale in heterogeneous and anisotropic formations. This correlation can then be used in assessment of water saturation. The sections below review the problem, present specific research objectives, and provide a preview of the methods used in this thesis.

1.2 Statement of the Problem

Conventional resistivity-porosity-saturation models such as Archie's model (Archie 1942), dual-water model (Clavier et al. 1984), and Waxman-Smits model (Waxman and Smits 1968) correlate borehole electrical resistivity measurements to pore-scale petrophysical properties in conventional reservoirs. To predict petrophysical properties such as fluid saturation at different scales (i.e., pore-scale and log-scale), a persistent

correlation must exist between physical properties (e.g., electrical resistivity) and petrophysical properties (e.g., porosity) at those scales. However, these correlations do not persist in rocks with complex pore structure and fabric (e.g., laminated shaly-sand formations and carbonate formations) due to the heterogeneity and anisotropy that causes variations in the measurements of physical and petrophysical properties at different scales (Knackstedt et al. 2005). Thus, correlations that persist at a certain scale in homogeneous formations are not reliable methods to estimate petrophysical properties in general. These correlations will incur uncertainties when applied to heterogeneous and anisotropic formations.

Previous work showed that the electrical resistivity measurements are not only affected by volumetric concentration of conductive components (i.e., formation water and pyrite) but also by the directional connectivity of these components (Chen et al. 2014). However, the relationship between directional connectivity of conductive components in anisotropic and complex formations and electrical resistivity at different scales (i.e., pore-scale and log-scale) has yet to be thoroughly understood. This thesis aims to find a persistent correlation at different scales in heterogonous and anisotropic formations. The following section states the specific research objectives of this thesis.

1.3 Research Objectives

To address the need for a reliable correlation to estimate petrophysical properties (e.g., fluid saturation and porosity) at different scales (i.e., log-scale and pore-scale), this research focuses on (a) quantifying directional connectivity tensor at different scales using

numerical simulations, (b) investigating the persistence of a relationship between electrical resistivity and the directional connectivity tensor at different micro-scales in heterogeneous and anisotropic rocks, and (c) applying this relationship in assessment of water saturation.

The methods designed to achieve these research objectives include using micro-CT (Computed Tomography) scan images from variable rock types and estimating physical and petrophysical properties at different scales (i.e., pore-scales). These methods are explained in detail in the following section.

2. METHOD

This section first explains the pixel-based segmentation process of the 3D micro-CT images of the rocks used in this thesis. These 3D images then serve as inputs to the numerical simulations to estimate the different properties (i.e., electrical resistivity, porosity, and directional tortuosity). Next, the methods used to estimate the directional connectivity tensor, introduced by Chen and Heidari (2015), and directional tortuosity are explained. Afterwards, the method used in the estimation of effective electrical resistivity of the samples is discussed, followed by sample resizing which is used to reduce the computational time required to run the numerical simulations. Finally, this section presents the method proposed for the assessment of water saturation.

2.1 Pixel-Based Segmentation of Micro-CT Images

The pore-scale images of the carbonate and sandstone samples used in this thesis are acquired from two sources: the Petroleum Engineering and Rock Mechanics Group at Imperial College London, and a carbonate field. The grey-scale micro-CT images were then segmented and binarized using a Trainable Segmentation in ImageJ (Schneider et al. 2012). The images were then stacked and converted to a 3D data matrix including 0s and 1s (0 represents grain pixel and 1 represents pore pixel). **Figures 1** and **2** represent a two-dimensional (2D) slice of a sandstone micro-CT image before and after segmentation, respectively. Afterwards, all the samples were divided into subsamples at smaller sizes and then served as input for tortuosity, directional connectivity, and electrical resistivity estimation (**Figure 3**).

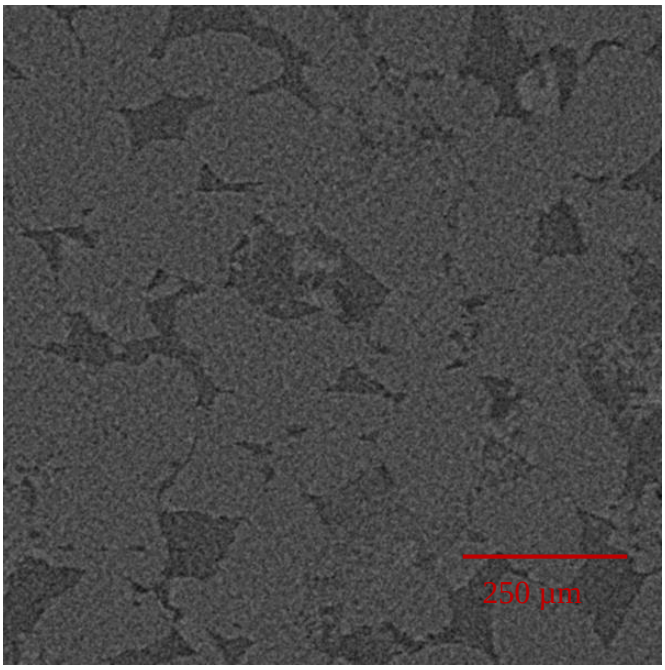

Figure 1: Raw 2D micro-CT image of a sandstone sample.

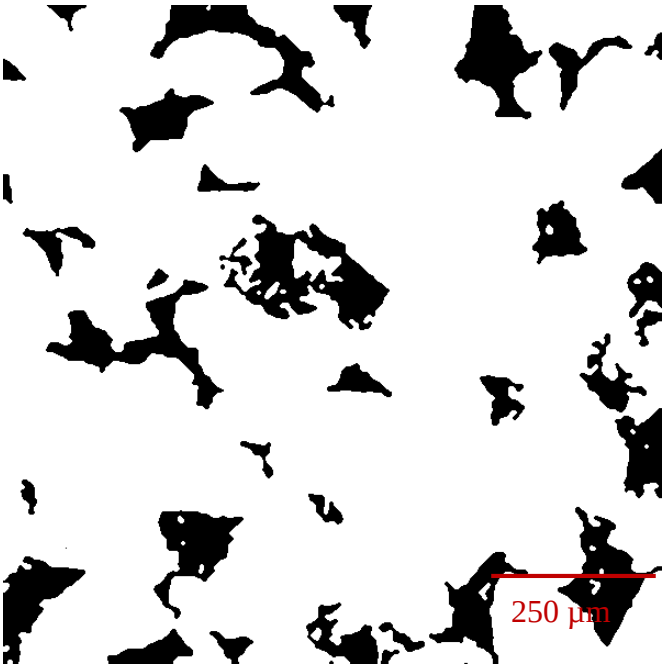

Figure 2: Binarized 2D micro-CT image of a sandstone sample. White and black regions represent grains and pore space, respectively.

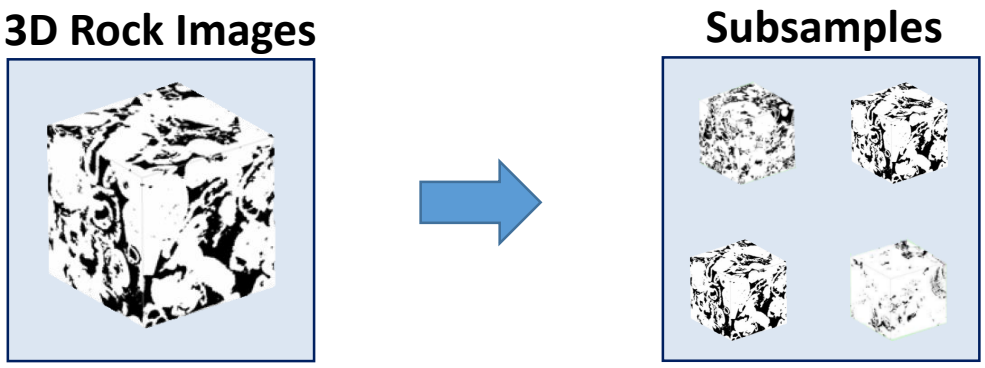

Figure 3: 3D binarized image divided into smaller subsamples where they are used as inputs to estimate different petrophysical properties.

2.2 Estimation of Tortuosity and Directional Connectivity

Tortuosity is a reliable indication of the heterogeneity and anisotropy of rock samples (Pfleiderer and Halls 1990; Siegesmund et al. 1991). The algorithm used in this thesis to estimate tortuosity was introduced by Nakashima and Kamiya (2007). It uses 3D micro-CT segmented images as the input. This algorithm **Figure 4** generates random walkers in the percolated pore space for a specific time, t. The directional-mean square displacement covered by random walkers is given by

$$\langle i(t)^2 \rangle = \frac{1}{n}\sum_{k=1}^{n}(i_k(t) - i_k(0))^2 \,, \tag{3}$$

where i_k denotes the position of the k^{th} random walker in the i^{th} direction at time t and n is the total number of random walkers used in the algorithm. The total mean-square displacement is given by

$$\langle r(t)^2 \rangle = \langle x(t)^2 \rangle + \langle y(t)^2 \rangle + \langle z(t)^2 \rangle . \quad (4)$$

In order to estimate the tortuosity, the time derivative of the displacement covered by the walkers is used. The tortuosity is given by

$$\tau = \frac{h^2 dt}{d\langle r(t)^2 \rangle}, \quad (5)$$

where τ is the dimensionless tortuosity, h is the dimension of the cubic voxel, and $(d(r(t)^2)/dt)$ is the rate of change of the total mean-square displacement with respect to time.

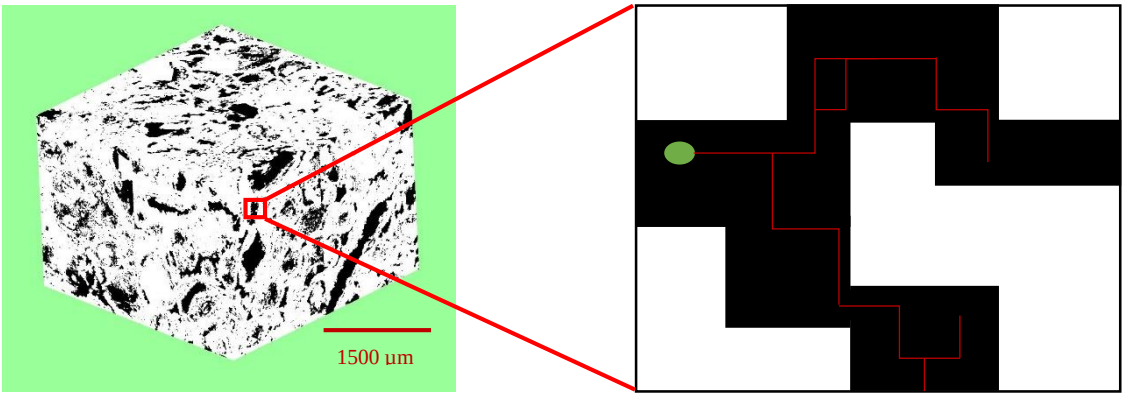

Figure 4: Elaboration of the random walk algorithm. The left image is the 3D sample with black and white representing pore and grain, respectively. The right image shows the path of the random walker in the pore.

Chen and Heidari (2015) proposed a new directional connectivity tensor expressed as a function of volumetric concentration of conducting components and their tortuosity. The directional connectivity tensor is defined as

$$\Psi_j = \sum_{k=1}^{m} \frac{C_k}{\tau_{k,j}^{\alpha}}, \quad (6)$$

where m is the total number of the connected conductive clusters (e.g., formation water and pyrite), α is a sample dependent connectivity parameter, C_k is the volumetric concentration of the k^{th} connected conductive cluster, and $\tau_{k,j}$ is the directional tortuosity in the j^{th} direction of the k^{th} connected conductive cluster. In partially water-saturated samples, C_k is defined as the product of porosity and water saturation for the pore network.

2.3 Numerical Estimation of Effective Electrical Resistivity

The 3D micro-CT images of the field samples and subsamples serve as inputs for the numerical simulation which estimates the electric potential distribution. For the case where the electric potential is independent of time, it must satisfy the Laplace's equation given by

$$\nabla \cdot (\sigma \nabla U) = 0, \quad (7)$$

where σ is the electrical conductivity and U is the electric potential. To calculate the electric potential distribution, Laplace's equation is numerically solved using a finite difference approach. The numerical solver was developed by Chen et al. (2014). The differential form of Ohm's law then helps to estimate effective electrical resistivity of the samples and subsamples. **Table 3** summarizes the resistivity values assumed for the rock components in the numerical simulations.

Table 3: Assumed Electrical Resistivity of The Rock Components in The Numerical Simulations

Rock components	Electrical resistivity at 175 ^{o}F (ohm-m)
Hydrocarbon	10^7
Grains	10^7
Formation Water	0.05

After estimating electrical resistivity, formation factor was estimated (*FF*) via

$$FF_j = \frac{(R_T)_j}{R_w}, \tag{8}$$

where FF_j is the formation factor in the j^{th} direction, $(R_T)_j$ is the bulk electrical resistivity of the rock-fluid system in the j^{th} direction, and R_w is the formation water electrical resistivity.

2.4 Sample Resizing

Electrical resistivity and tortuosity were estimated using numerical simulations. All the numerical simulations were conducted with the supercomputing facility at Texas A&M University, with 3168-core IBM (iDatePlex) and 372 nodes. Each node is a 64-bit shared-memory multi-processor system. The computational time needed to estimate electrical resistivity is directly proportional to both the size and complexity of the sample (**Figure 5**). A sample size of 256^3 pixel can take up to 72 hours to run in the Texas A&M supercomputing facility.

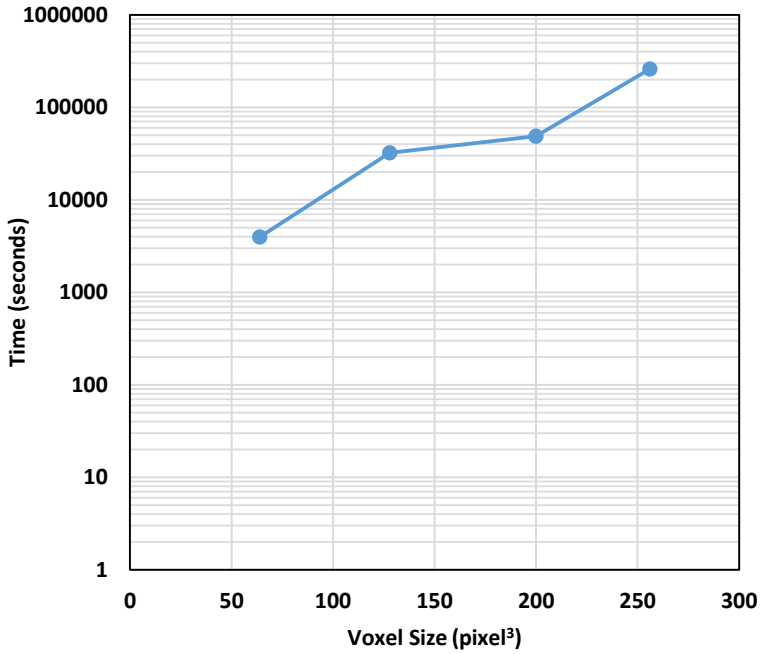

Figure 5: Sample size (x-axis) plotted against computational time in the Texas A&M supercomputing facility (y-axis) to estimate electrical resistivity of 3D samples.

On the other hand, the voxel size of the largest sample size used in this thesis is 1320x1320x931. To overcome the problem of the long computational time required for large samples, sample resizing was introduced. The purpose of sample resizing is to decrease the voxel size of a large sample, by using some sort of averaging, without changing the physical and petrophysical properties of the samples (i.e., porosity, electrical resistivity and tortuosity). Bakke et al. (2007) showed that the same sample with different resolutions can have similar physical and petrophysical properties, as long as the two resolutions are not very different from each other. Resizing was performed using ImageJ (Schneider et al. 2012). Resizing in ImageJ can be performed with or without

interpolation. ImageJ has two built-in interpolation methods, bilinear and bicubic. To identify the best method for resizing, physical and petrophysical properties of the original samples and the resized samples were compared. **Figures 6** and **7** compare the porosity and formation factor, respectively, between the actual samples and the resized samples. In the comparison, resizing was first done without interpolation, then the two interpolation methods were used. The bicubic interpolation method provided the closest estimation of the physical and petrophysical properties of the resized 3D rock images compared to the original images. This resizing method was used throughout the rest of this thesis for samples of voxel size larger than 256^3.

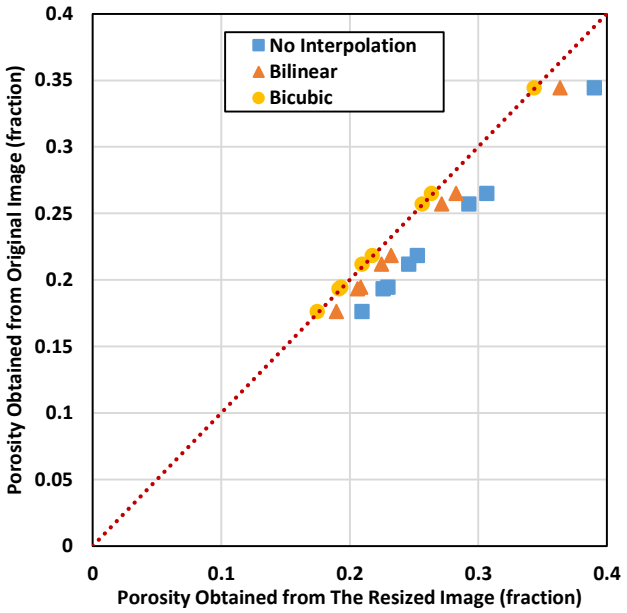

Figure 6: Comparison between the porosity of the original images and the resized images.

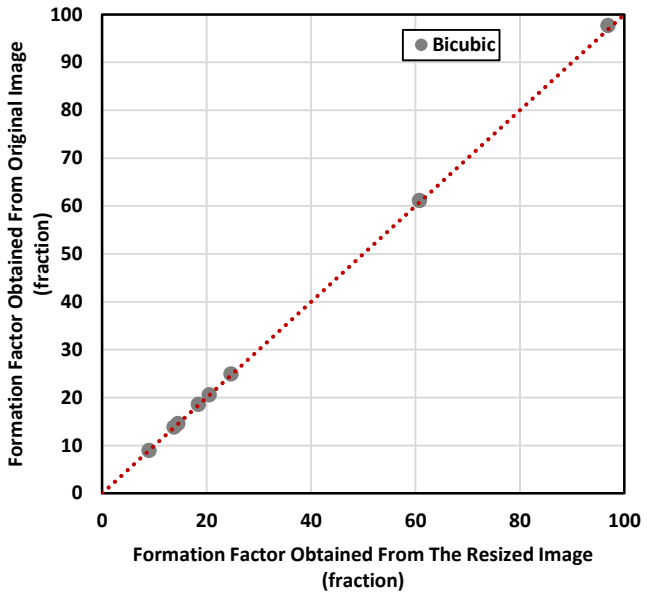

Figure 7: Comparison between the formation factor of the original images and the resized images.

2.5 Assessment of Water Saturation

One of the goals of this thesis is to propose a relationship between formation factor and directional connectivity that persists at different micro-scales in heterogeneous and anisotropic rocks. This relationship is intended to be used in the assessment of water saturation in the pore-scale. **Figure 8** is a flowchart that describes the proposed steps for the assessment of water saturation using the proposed relationship.

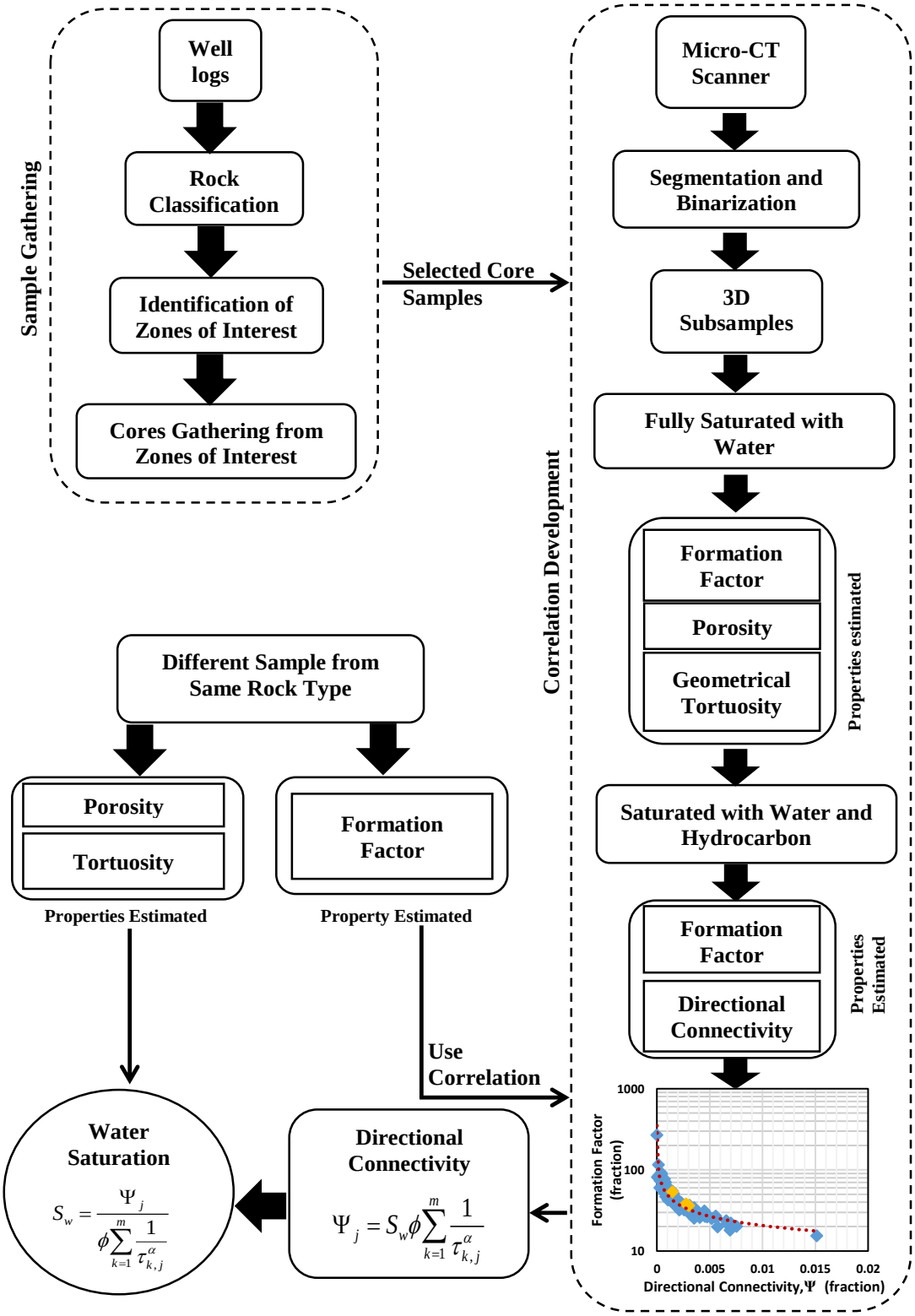

Figure 8: Workflow recommended to be used for assessment of water saturation.

3. RESULTS

This section documents the results of the numerical simulations used to investigate a persistent relationship between formation factor and directional connectivity at different sample sizes. First, an investigation was conducted to show how the formation factor varied as a function of porosity at different subsample sizes in six samples fully and partially saturated with water. Second, the variation of formation factor as a function of directional connectivity was investigated for the six samples with full and partial water saturation.

3.1 Application to Carbonate and Sandstone Samples

Six carbonate and sandstone samples were analyzed. **Table 4** summarizes the properties of the samples and the subsamples in this thesis. **Figures 9** through **14** show the 3D pore-scale micro-CT image of the six samples. The first five samples in **Table 4** were obtained from the Petroleum Engineering and Rock Mechanics Group at Imperial College London (Dong 2007).

Table 4: Properties of Six Carbonate and Sandstone Samples

Sample	Voxel size (pixels^3)	Resolution (μm/pixel)	Porosity (%)	Subsample sizes (pixels^3)
Sandstone sample no. 1	300x300x300	8.6	23.3	150^3, 200^3, and 300^3
Sandstone sample no. 2	400x400x400	5.35	19.5	300^3 and 200^3
Carbonate sample no. 1	1024x1024x1024	2.65	15	512^3 and 256^3
Carbonate sample no. 2	400x400x400	2.85	23.3	150^3, 200^3, and 300^3
Carbonate sample no. 3	400x400x400	5.35	16.8	150^3, 200^3, and 300^3
Carbonate sample no. 4	1320x1320x931	2.5	17.7	233^3 and 466^3

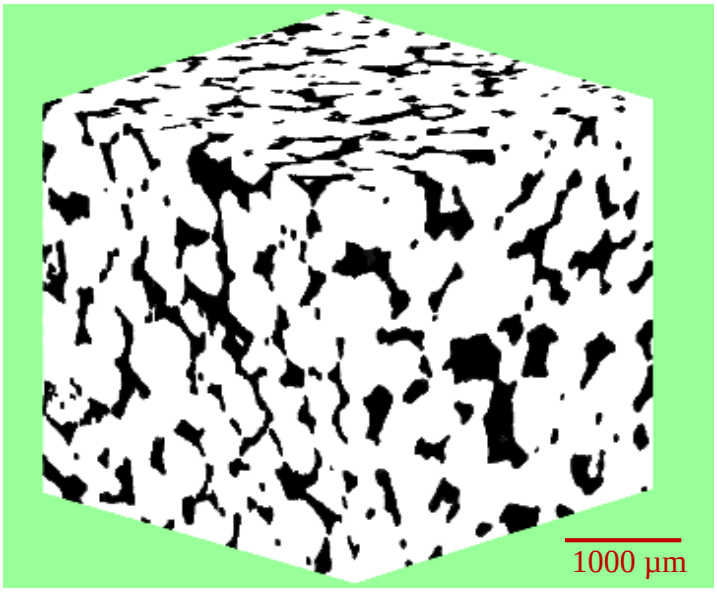

Figure 9: The 3D pore-scale image of sandstone sample no. 1. White and black regions represent grains and pore space, respectively.

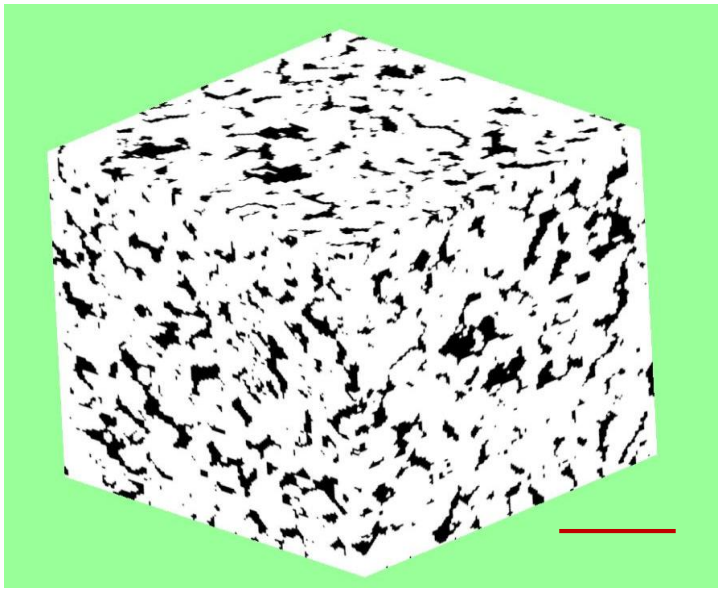

Figure 10: The 3D pore-scale image of sandstone sample no. 2. White and black regions represent grains and pore space, respectively.

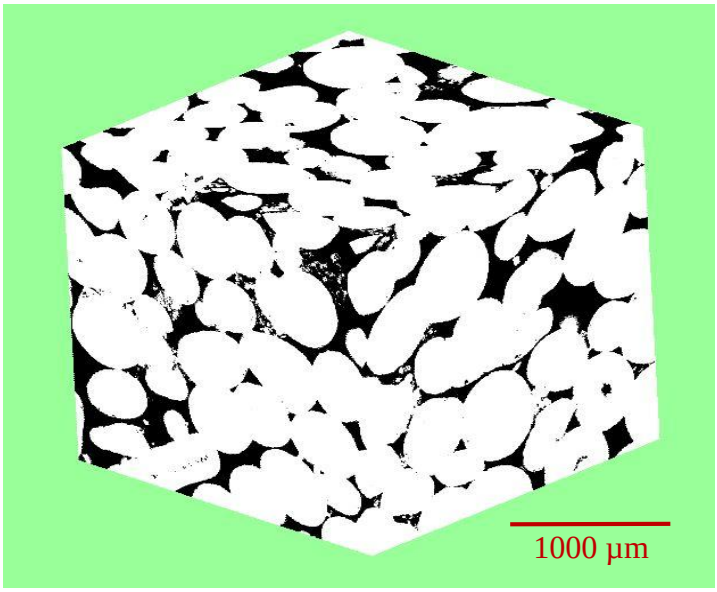

Figure 11: The 3D pore-scale image of carbonate sample no. 1. White and black regions represent grains and pore space, respectively.

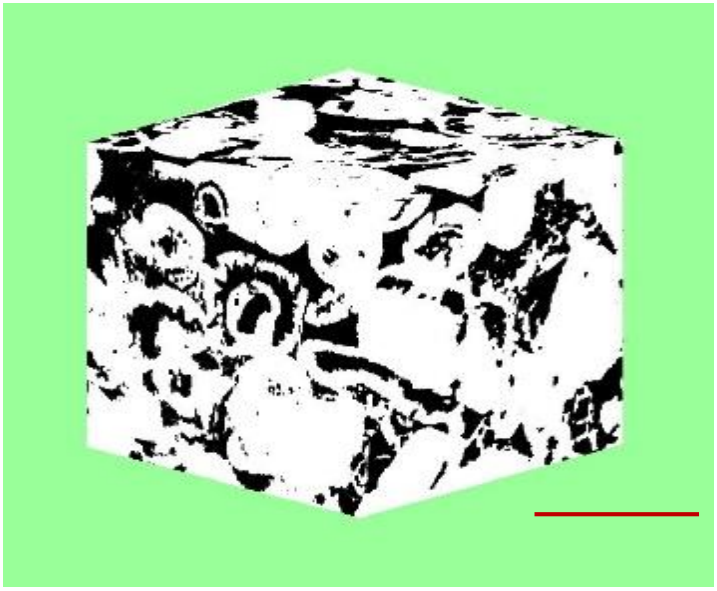

Figure 12: The 3D pore-scale images of carbonate sample no. 2. White and black regions represent grains and pore space, respectively.

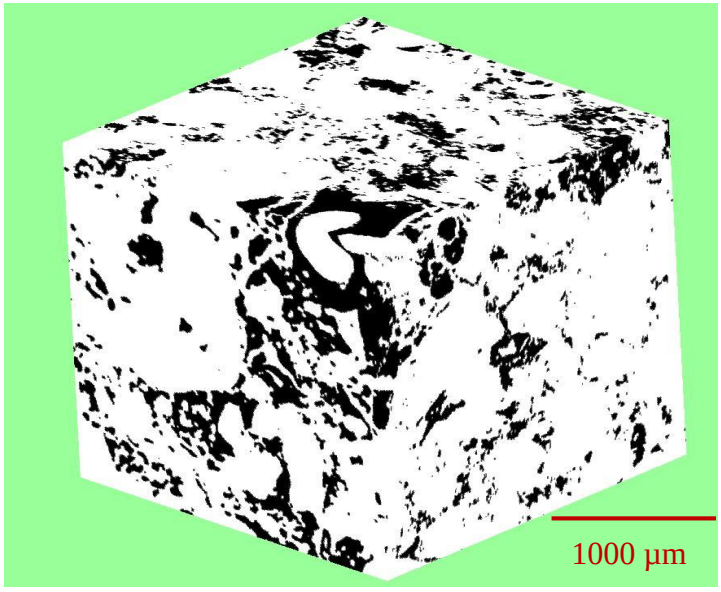

Figure 13: The 3D pore-scale images of carbonate sample no. 3. White and black regions represent grains and pore space, respectively.

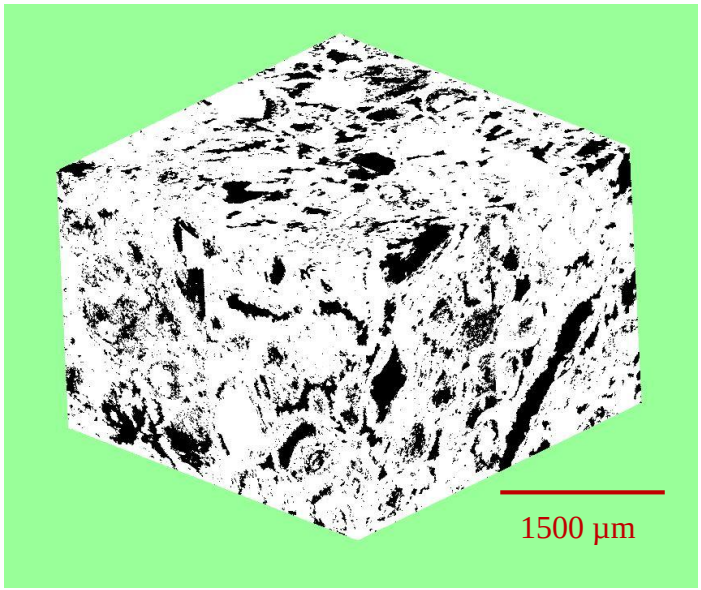

Figure 14: The 3D pore-scale images of carbonate sample no. 4. White and black regions represent grains and pore space, respectively.

3.1.1 Fully Water-Saturated Samples

The samples were first saturated with water. Then, porosity was estimated for all the samples and subsamples. Afterwards, the formation factor was estimated. Finally, the directional connectivity was estimated. The following is a summary of the results of the first five samples.

Figures 15, **17**, **19**, **21**, and **23** illustrate the estimated formation factor from numerical simulations plotted against porosity for the subsamples taken at different scales in sandstone and carbonate samples. The relationship between formation factor and porosity provides a weak correlation. However, a stronger correlation is observed (improvement of 59% in correlation coefficient) between formation factor and directional connectivity (**Figures 16**, **18**, **20**, **22**, and **24**) compared to the relationship between formation factor and porosity.

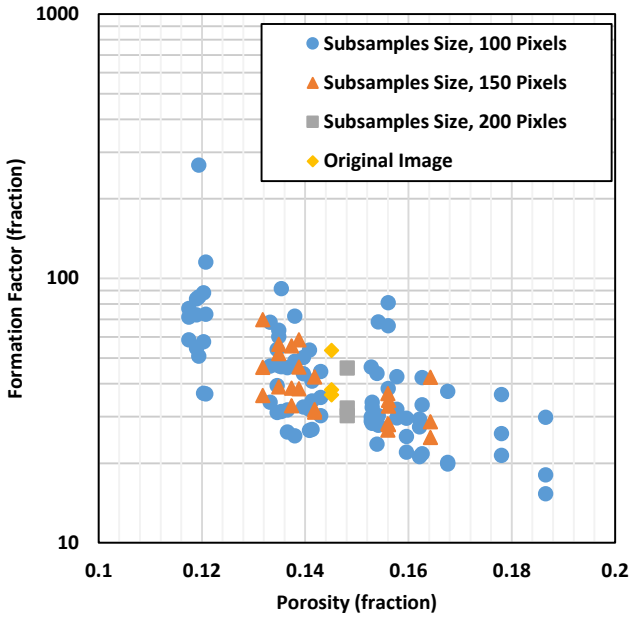

Figure 15: Sandstone sample no. 1: Formation factor plotted against porosity at different scales. All the rock samples are fully water-saturated.

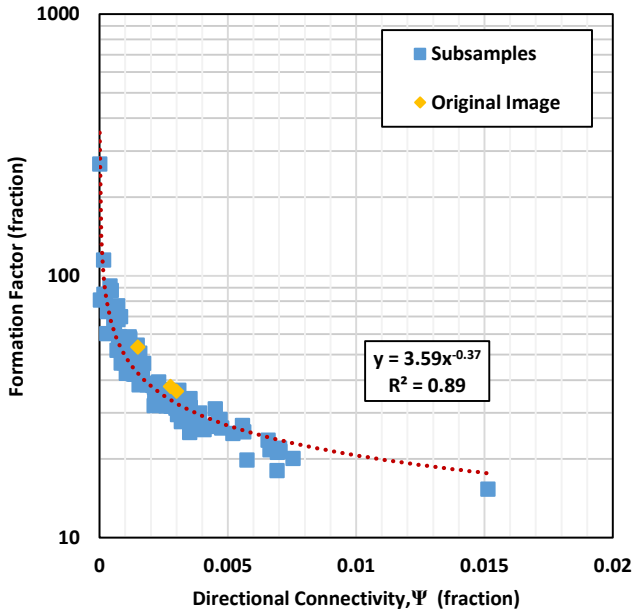

Figure 16: Sandstone sample no. 1: Formation factor plotted against directional connectivity tensor at different scales. All the rock samples are fully water-saturated.

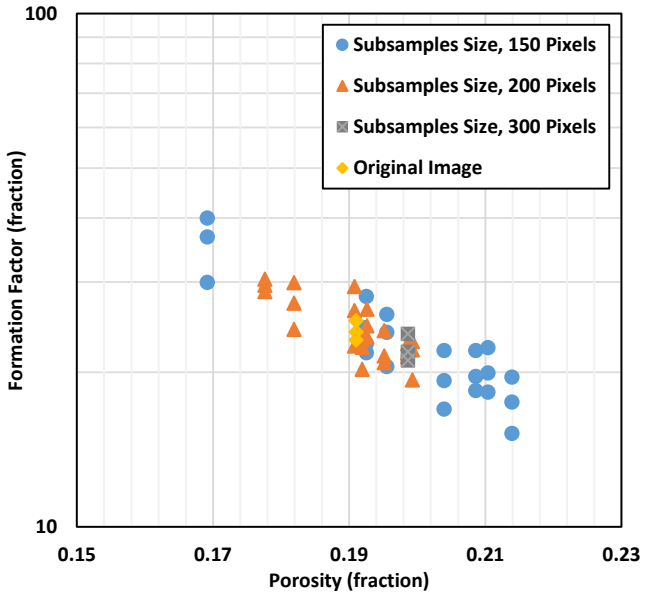

Figure 17 : Sandstone sample no. 2: Formation factor plotted against porosity at different scales. All the rock samples are fully water-saturated.

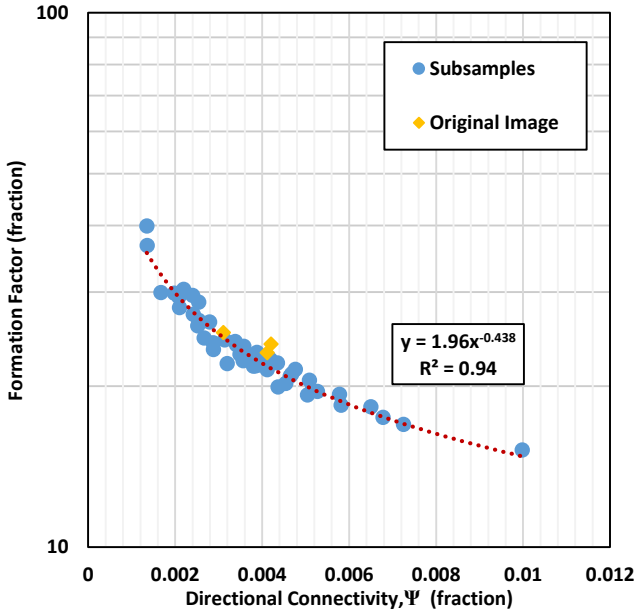

Figure 18: Sandstone sample no. 2: Formation factor plotted against directional connectivity tensor at different scales. All the rock samples are fully water-saturated.

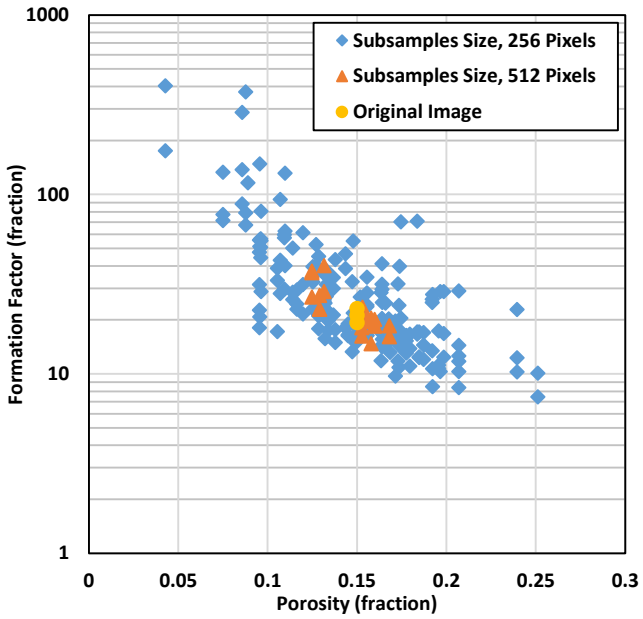

Figure 19: Carbonate sample no. 1: Formation factor plotted against porosity at different scales. All the rock samples are fully water-saturated.

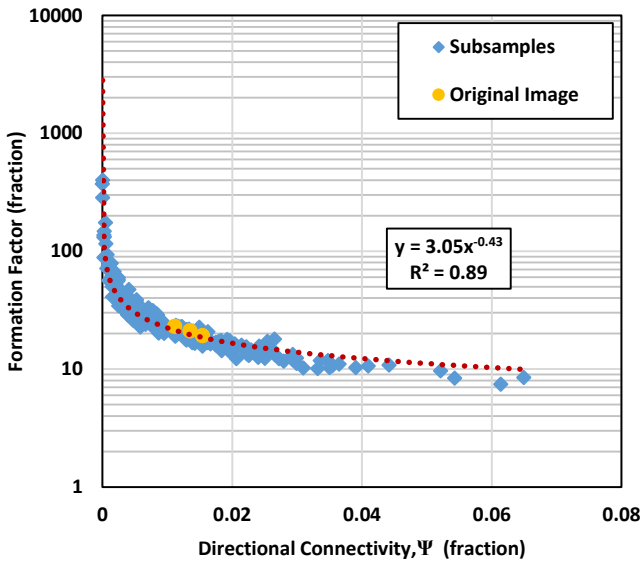

Figure 20: Carbonate sample no. 1: Formation factor plotted against directional connectivity tensor at different scales. All the rock samples are fully water-saturated.

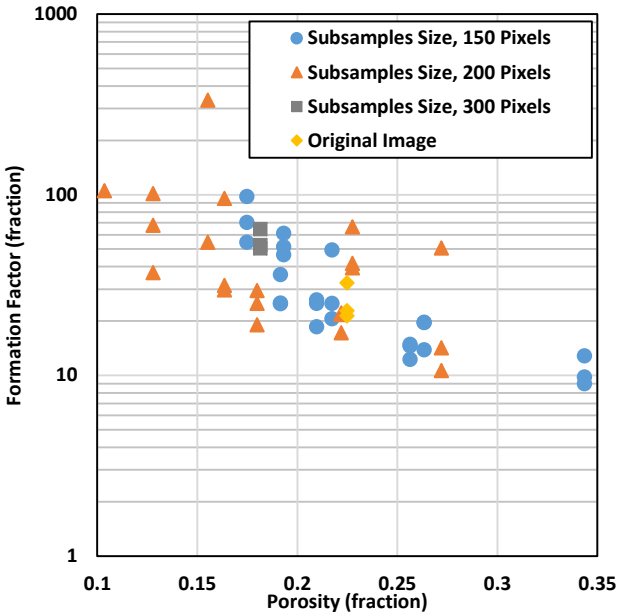

Figure 21: Carbonate sample no. 2: Formation factor plotted against porosity at different scales. All the rock samples are fully water-saturated.

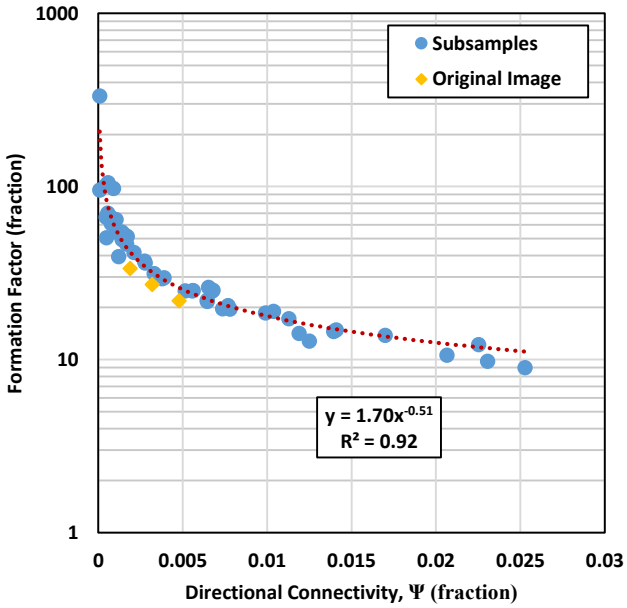

Figure 22: Carbonate sample no. 2: Formation factor plotted against directional connectivity tensor at different scales. All the rock samples are fully water-saturated.

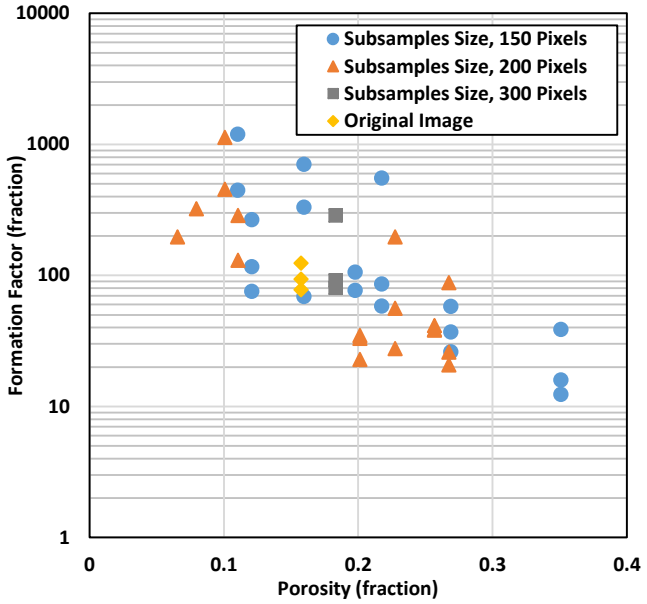

Figure 23: Carbonate sample no. 3: Formation factor plotted against porosity at different scales. All the rock samples are fully water-saturated.

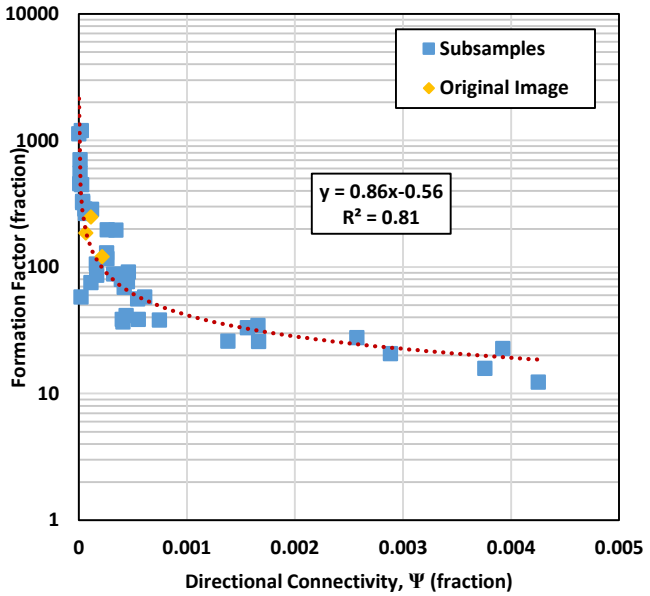

Figure 24: Carbonate sample no. 3: Formation factor plotted against directional connectivity tensor at different scales. All the rock samples are fully water-saturated.

3.1.2 Partially Water-Saturated Rock Samples

All the samples were then saturated with both water and hydrocarbon. Afterwards, the formation factor and the directional connectivity were estimated. The following is a summary of the results obtained.

Table 5 summarizes hydrocarbon saturation for the six samples. **Figures 25**, **27**, **29**, **31**, and **33** show the estimated formation factor from numerical simulations plotted against porosity for the subsamples taken at different scales in the first five samples. **Figures 26**, **28**, **30**, **32**, and **34** illustrate the estimated formation factor from numerical simulations plotted against directional connectivity for the subsamples taken at different scales in the first five samples. A stronger correlation was observed (improvement of 54% in correlation coefficient) between formation factor and directional connectivity compared to the correlation between formation factor and porosity.

In addition to the previously tested rock samples, this section includes the results for another heterogeneous and anisotropic carbonate sample, carbonate sample no. 4. **Figures 35** and **36** show the resulting plot of formation factor against porosity and directional connectivity, respectively, in carbonate sample no. 4 for both fully- and partially-saturated samples. A stronger correlation was observed (improvement of 52% in correlation coefficient) between formation factor and directional connectivity, compared to the correlation between formation factor and porosity in carbonate sample no. 4.

Table 5: Hydrocarbon Saturation in Six Samples	
Sample	Hydrocarbon saturation (%)
Sandstone sample no. 1	13
Sandstone sample no. 2	10
Carbonate sample no. 1	51
Carbonate sample no. 2	36
Carbonate sample no. 3	21
Carbonate sample no. 4	32

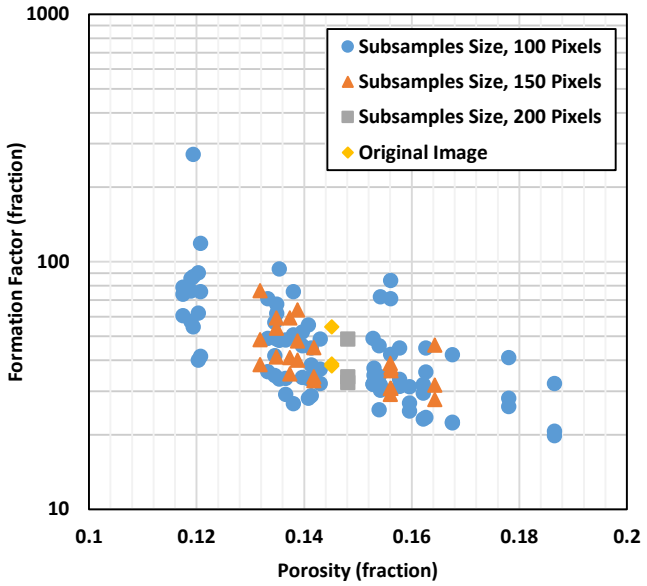

Figure 25: Sandstone sample no. 1: Formation factor plotted against porosity at different scales. Water saturation is 87% in the original sample.

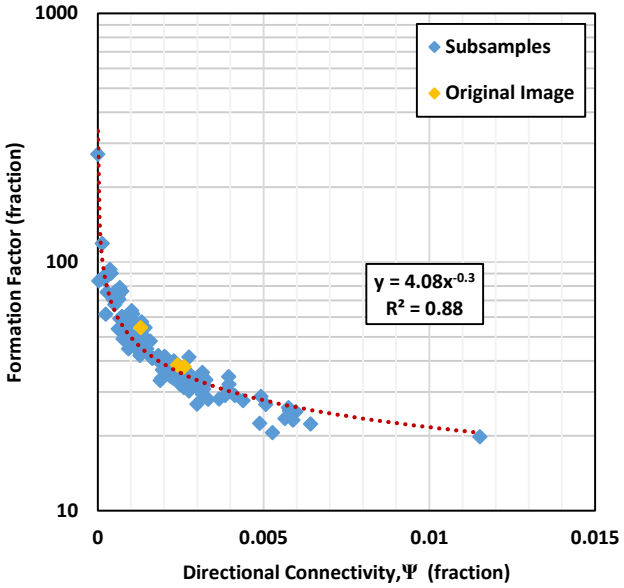

Figure 26: Sandstone sample no. 1: Formation factor plotted against directional connectivity tensor at different scales. Water saturation is 87% in the original sample.

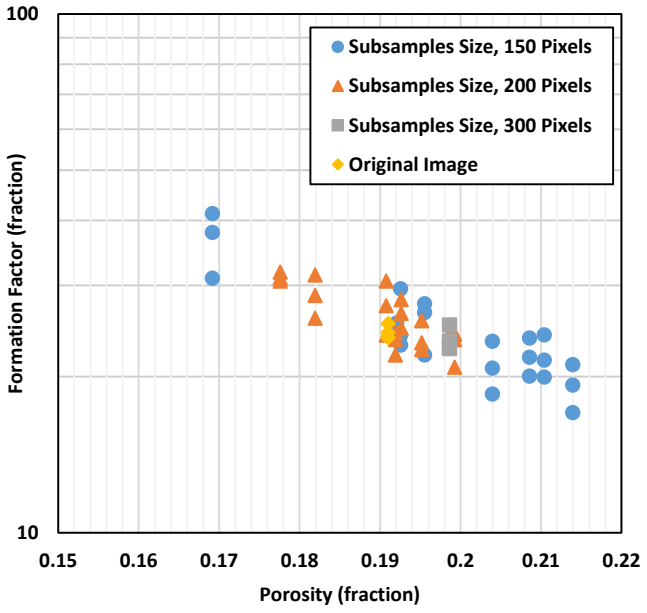

Figure 27: Sandstone sample no. 2: Formation factor plotted against porosity at different scales. Water saturation is 90% in the original sample.

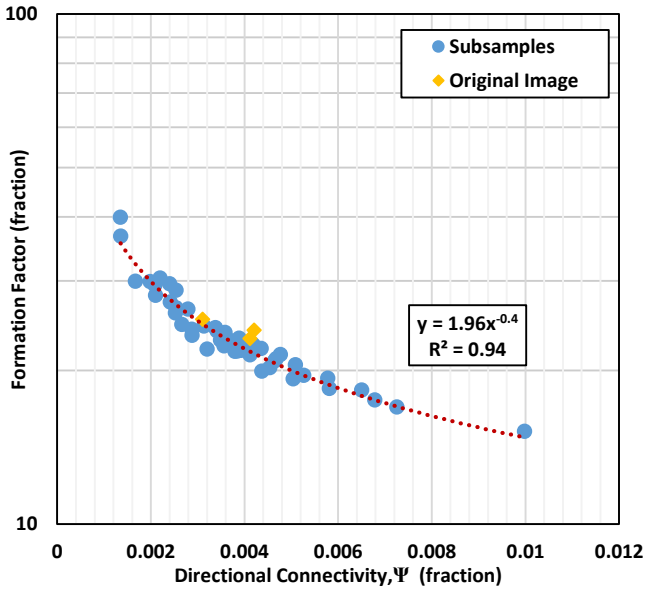

Figure 28: Sandstone sample no. 2: Formation factor plotted against directional connectivity tensor at different scales. Water saturation is 90% in the original sample.

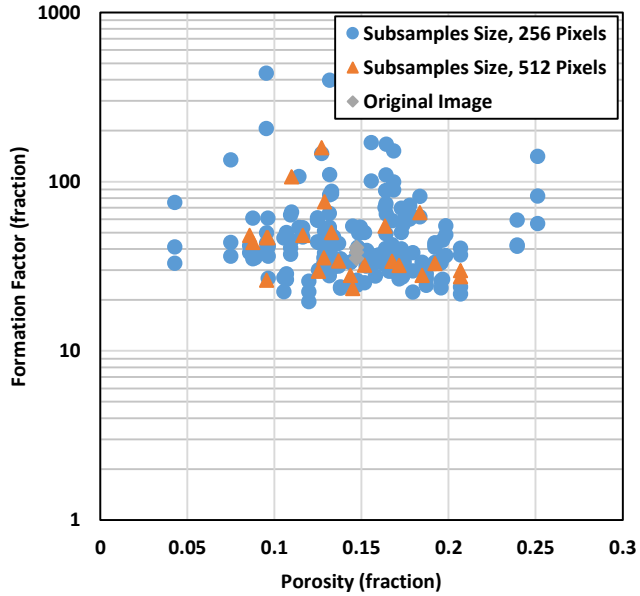

Figure 29: Carbonate sample no. 1: Formation factor plotted against porosity at different scales. Water saturation is 49% in the original sample.

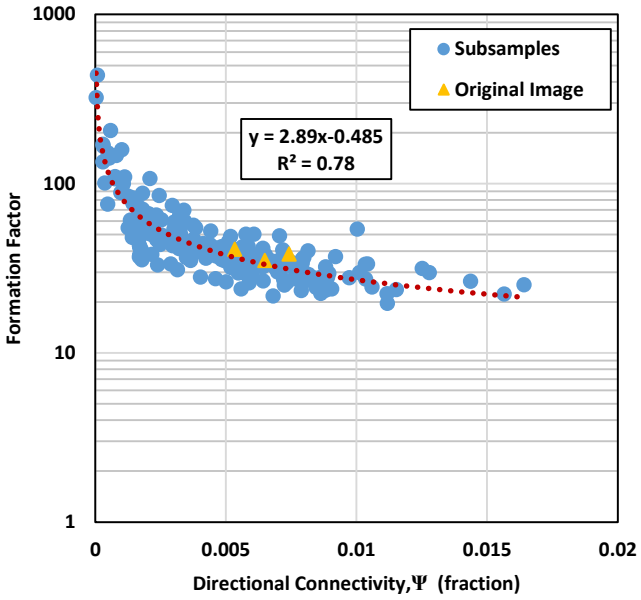

Figure 30: Carbonate sample no. 1: Formation factor plotted against directional connectivity tensor at different scales. Water saturation is 49% in the original sample.

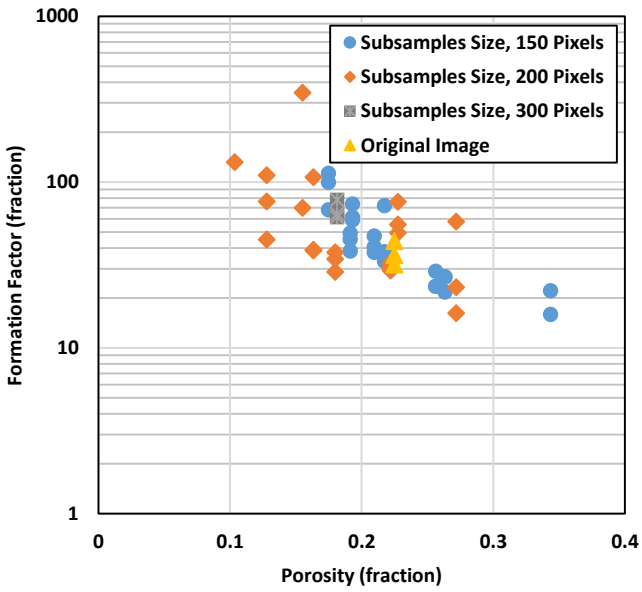

Figure 31: Carbonate sample no. 2: Formation factor plotted against porosity at different scales. Water saturation is 64% in the original sample.

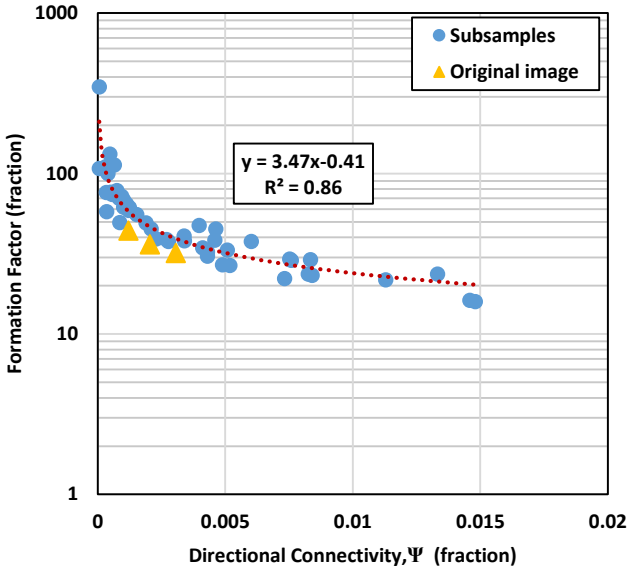

Figure 32: Carbonate sample no. 2: Formation factor plotted against directional connectivity tensor at different scales. Water saturation is 64% in the original sample.

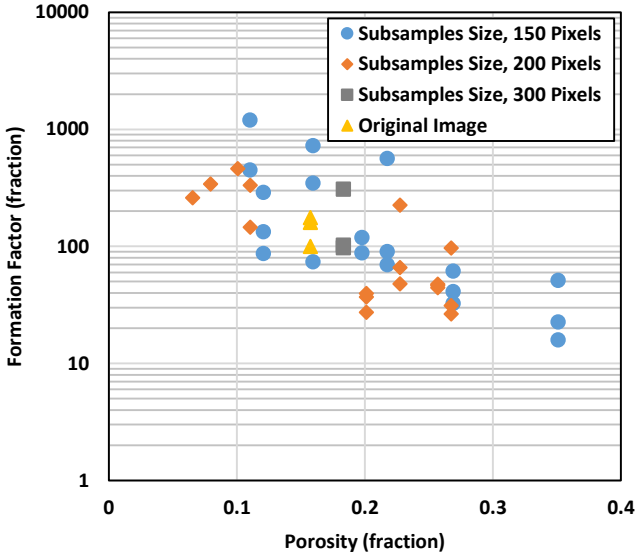

Figure 33: Carbonate sample no. 3: Formation factor plotted against porosity at different scales. Water saturation is 79% in the original sample.

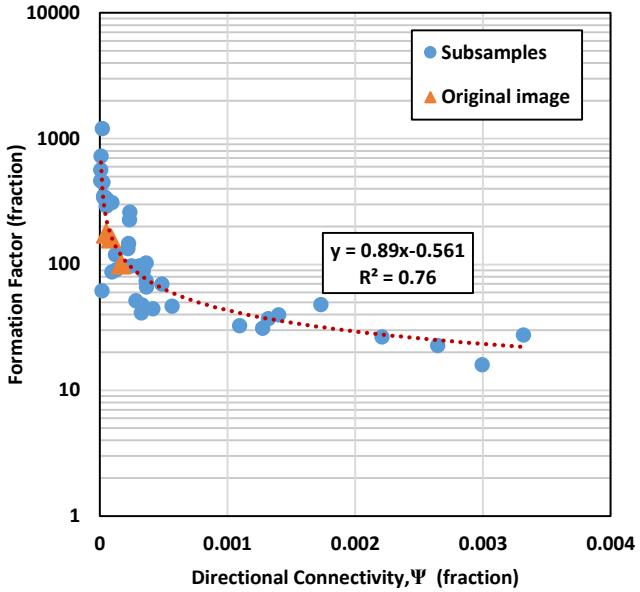

Figure 34: Carbonate sample no. 3: Formation factor plotted against directional connectivity tensor at different scales. Water saturation is 79% in the original sample.

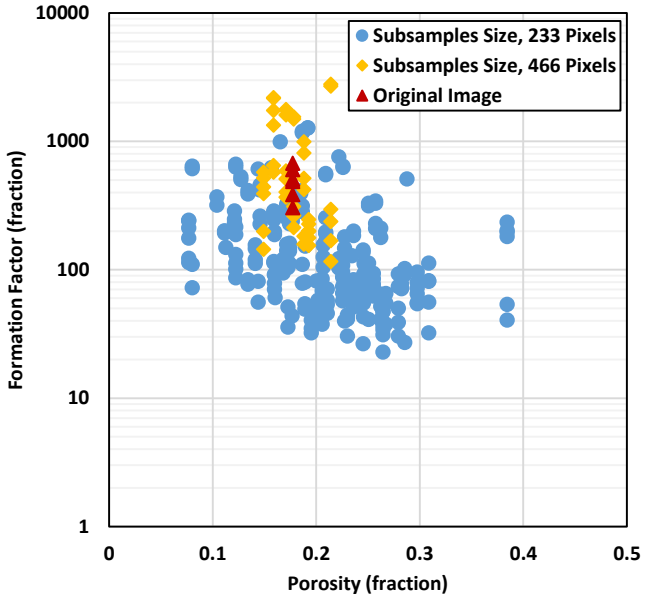

Figure 35: Carbonate sample no. 4: Formation factor plotted against porosity at different scales. Some of the rock samples are fully water-saturated, others are partially water-saturated.

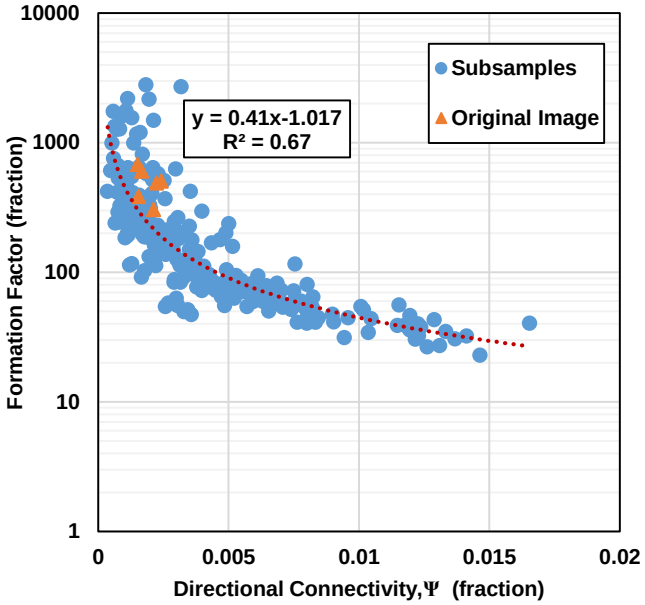

Figure 36: Carbonate sample no. 4: Formation factor plotted against directional connectivity tensor at different scales. Some of the rock samples are fully water-saturated, others are partially water-saturated.

3.2 Assessment of Water Saturation

To illustrate how incorporating directional connectivity can improve water saturation estimation, the proposed method was applied in subsamples from carbonate sample no. 4. A comparison was performed between the modified Archie's model, which is discussed in Winsauer et al. (1952) (**Table 2**), and the introduced method. This conventional model is referred to as Archie's model in this subsection. The *a*, *m*, and *n* parameters were estimated using the subsamples fully saturated with water, which provided the values 1.2, 2.3, and 2.4, respectively. The *a*, *m*, and *n* values were assumed to be the same for the original image and all the subsamples. **Figure 37** illustrates the comparison between the actual water saturation and the estimated water saturation using Archie's model.

Afterwards, a comparison was performed between the actual water saturation and the estimated water saturation using the introduced method (**Figure 38**). The estimates of water saturation were improved by 50% when water saturation was estimated using the introduced method.

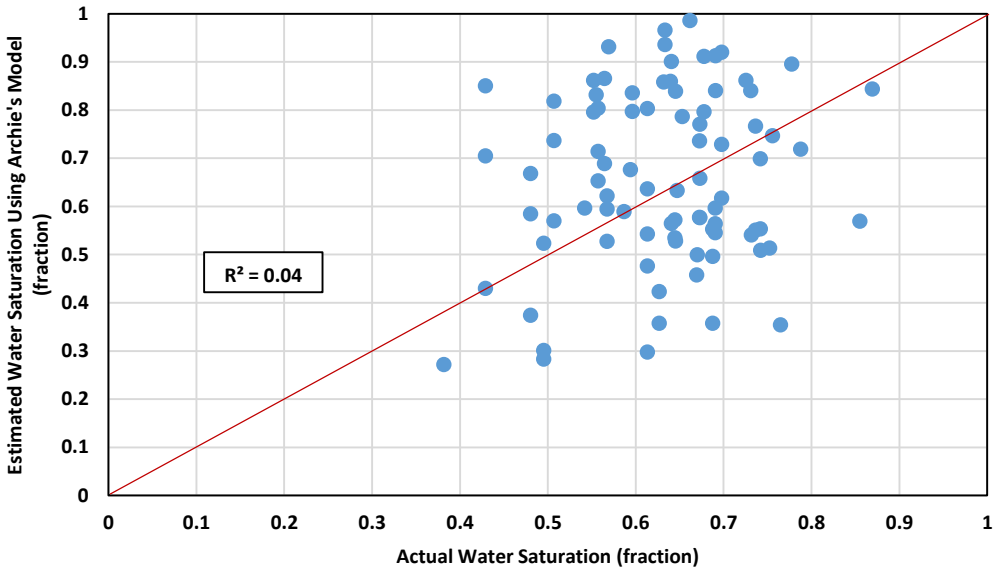

Figure 37: Carbonate sample no. 4: The estimated water saturation using Archie's model plotted against the actual water saturation in the subsamples.

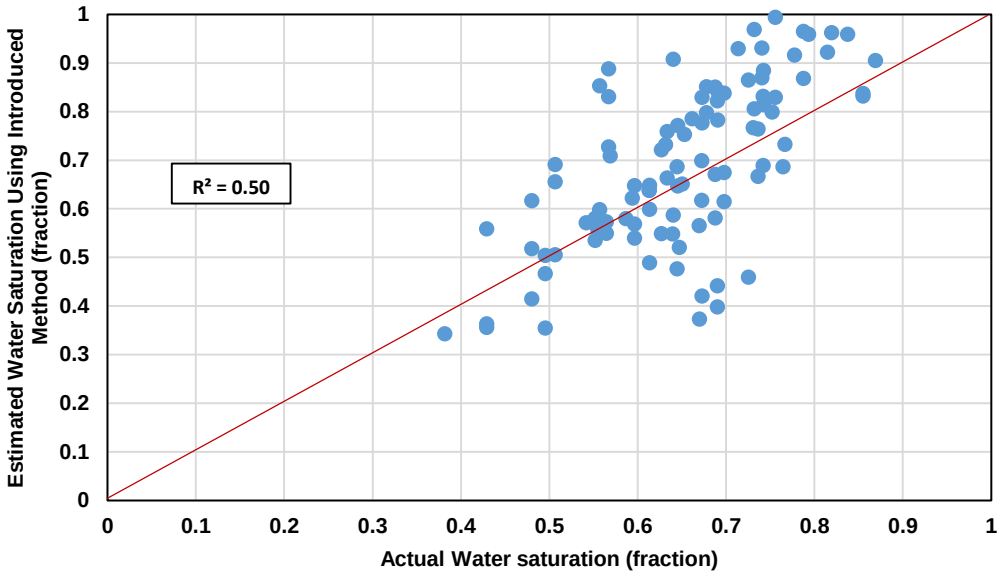

Figure 38: Carbonate sample no. 4: The estimated water saturation using the introduced method plotted against the actual water saturation in the subsamples.

4. SUMMARY AND CONCLUSIONS

This section is a summary of the work and results obtained in this thesis. It also presents the conclusions and recommendations for future work.

4.1 Summary

The main objectives of this thesis included:

- Quantifying the directional connectivity tensor at different scales in the presence of complex pore structure and anisotropy.
- Finding a relationship between directional connectivity and electrical resistivity that persists at different micro-scales in heterogeneous formations.
- Investigating the possibility of using the concept of scale-dependent pore-network connectivity in assessment of water saturation.

The aforementioned objectives were accomplished by analyzing micro-CT scan images in six rock samples from different rock types (i.e., sandstone and carbonate). The micro-CT scan images were segmented and binarized into pores and grains. Afterwards, the 3D pore-scale images of each sample were divided into smaller subsamples. Then, all the digital samples and subsamples were fully and then partially saturated with water. Porosity, formation factor, tortuosity, and directional connectivity were estimated for all the samples and subsamples. A stronger correlation between directional connectivity and electrical resistivity at different micro-scales was observed in the six samples, when compared to the conventional correlation between electrical resistivity and porosity.

4.2 Conclusions

This research involved a series of numerical simulations to find a consistent relationship between the directional connectivity and formation factor at different micro-scales in the presence of complex pore structure and anisotropy.

The conclusions that can be drawn from this research are as follows:

1. Conventional volumetric correlation between porosity and formation factor do not persist at different scales for heterogeneous and anisotropic rock samples studied in this thesis.
2. For fully water-saturated carbonate and sandstone samples, the correlation between directional connectivity and formation factor showed an improvement of up to 59% in the correlation coefficient compared to the correlation between formation factor and porosity.
3. For partially water-saturated samples, for the same set of samples, the correlation between directional connectivity and formation factor showed an improvement of up to 54% in the correlation coefficient compared to the correlation between formation factor and porosity.
4. The obtained relationship between directional connectivity and formation factor was used in estimating water saturation. An improvement of up to 50% in estimates of water saturation was observed, if the directional connectivity of the pore network is taken into account.

4.3 Recommendations

Although this thesis focused on finding a persistent relationship between formation factor and directional connectivity at different micro-scales, many problems of interpreting petrophysical properties at different scales remain unsolved.

A list of possible research avenues for future work that could expand the contributions of this thesis is presented below:

1. Apply the proposed method in organic-rich mudrocks where pore structure is more complex and there are more conductive components (i.e., pyrite, wet clays, and kerogen).

2. Conduct a comprehensive study of the nature of tortuosity and how to accurately estimate it at larger scales beyond the pore-scale.

3. Investigate the relationship between formation factor and directional connectivity in larger scales (e.g., log scales) and investigate the possibility of using this relationship in assessment of well-log-based water saturation.

REFERENCES

Alger, R. P., Raymer, L. L., Hoyle, W. R., and Tixier, M. P. 1963. Formation Density Log Applications in Liquid-Filled Holes. *SPE J.* **15** (3): 321-332.

Al-Omari, A. and Masad, E. 2004. Three dimensional simulation of fluid flow in X-ray CT images of porous media. *Int. J. Numer. Anal. Meth. Geomech.* **28** (1): 1327-1360.

Archie, G.E. 1942. The Electrical Resistivity Log as an Aid in Determining Some Reservoir Characteristics. *Transactions of the American Institute of Mining Metallurgical Engineers* (AIME) **146** (1): 54-62.

Armatas, S. 2006. Determination of the Effects of the Pore Size Distribution and Pore Connectivity Distribution on the Pore Tortuosity and Diffusive Transport in Model Porous Networks. *Chemical Engineering Science* **61** (14): 4662-4675.

Azegrouz, H., Trucco, E., Dhillon, B., MacGillivary, T., and MacCormick, I.J. 2006. Thickness Dependent Tortuosity Estimation for Retinal Blood Vessels. Presented at the 28th IEEE EMBS Annual International Conference, New York City, USA, 30 August - 3 September.

Bakke, S., Roth, S., Held, R. J., and Rueslatten H. G. 2007. Pore-Scale Modeling of Carbonate Reservoir Rocks. Presented at the International Symposium of the Society of Core Analysts, Calgary, Canada, 10-12 September.

Bardon, C. and Pied, B. 1969. Formation Water Saturation in Shaly Sands. Presented at SPWLA 10th Annual Logging Symposium, Houston, Texas, USA. 25-28 May.

Barrande, M., Bouchet, R., and Denoyel, R. 2007. Tortuosity of Porous Particles. *Analytical Chemistry* **79** (23): 9115-9121.

Bear, J. 1972. *Dynamics of Fluids in Porous Media*. Dover Publications.

Bear, J. and Bachmat, Y. 1990. *Introduction to Modeling of Transport Phenomena in Porous Media*. Dordrecht, Kluwer Academic Publishers.

Boudreau, B. and Meysman, J.R. 2006. Predicted Tortuosity of Muds. *Geology* **34** (8): 693-696.

Bowers M. and Fitz, D. 2000. A Probabilistic Approach to Determine Uncertainty in Calculated Water Saturation. Presented at the SPWLA 41st Annual Logging Symposium, Dallas, Texas, USA, 4-7 June.

Brace, W.F. and Orange A.S. 1966. Electrical Resistivity: Changes in Saturated Rock Due to Stress. *Science* **153**: 1525-1526.

Brace, W.F., Orange, A.S., and Madden T. M. 1965. The Effect of Pressure on the Electrical Resistivity of Water-Saturated Crystalline Rocks. *Journal of Geophysical Research* **70** (22): 5669-5678.

Brakel, J.V. and Heertjes, P.M. 1974. Analysis of Diffusion in Macroporous Media in Terms of Porosity, a Tortuosity and a Constrictivity Factor. *International Journal of Heat Transfer* **17**: 1093-1103.

Carman, P. C. 1937. Fluid Flow Though Granular Beds. *Transactions of the Institute of Chemical Engineers* **50**: 150-166.

Chapuis, R. and Gill, D. 1989. Hydraulic Anisotropy of Homogeneous Soils and Rocks: Influence of the Densification Process. *Bulletin of the International Association of Engineering Geology* **39** (1): 75-86.

Chatzis, I. and Dullien, F.A. L. 1985. The Modeling of Mercury Porosimetry and the Relative Permeability of Mercury in Sandstones using Percolation Theory. *Int. Chem. Eng.* **25**: 47-66.

Chen, H., Firdaus, G., and Heidari, Z. 2014. Impact of Anisotropic Nature of Organic-Rich Source Rocks on Electrical Resistivity Measurements. Presented at the SPWLA 55th Annual Well Logging Symposium, Abu Dhabi, UAE, 18-22 May.

Chen, H., Firdaus, G., and Heidari, Z. 2015. Quantifying the Directional Connectivity of Rock Constituents and its Impact on Electrical Resistivity of Organic-Rich Mudrocks. *Mathematical Geosciences*: doi: 10.1007/s11004-015-9595-9.

Chen, H. and Heidari, Z. 2014. Pore-Scale Evaluation of Dielectric Measurements in Formations with Complex Pore and Grain Structures. *Petrophysics* **55** (6): 587-597.

Clavier, C., Coates, G., and Dumanoir, J. 1984. Theoretical and Experimental Bases for The Dual water Model for Interpretation of Shaly Sands. *SPE J.* **24** (2): 153-168.

Clennell, M.B. 1997. Tortuosity: A Guide Through the Maze. *Geological Society London Special Publications* **122**: 299-344.

Comiti, J. 1989. A New Model for Determining Mean Structure Parameters of Fixed Beds from Pressure Drop Measurements: Application to Beds Packed with Parallelepipedal Particles. *Chemical Engineering Science* **44** (7): 1539-1545.

Cornell, D. Katz, D.L. 1953. Flow of Gases Through Consolidated Media. *Industrial and Engineering Chemistry* **45**: 2145-2152.

De Witte, A.J. 1957. Saturation and Porosity from Electric Logs in Shaly Sands. *Oil & Gas J.* **55** (4): 115-121.

De Witte, L. 1955. A Study of Electric Log Interpretation Methods in Shaly Formations. SPE.

Dias, R., Teixeira, A., and Mota, M. 2006. Tortuosity Variation in a Low Density Binary Particulate Bed. *Separation and Purification Technology* **51** (2): 180-184.

Diederix, K.M. 1982. Anomalous Relationships Between Resistivity Index and Water Saturations in the Rotliegend Sandstone (The Netherlands). Presented at the SPWLA 23rd Annual Logging Symposium, Corpus Christi, Texas, USA, 6-9 July.

Diniz-Ferreira, E.L. and Torres-Verdín, C., 2012. Improved Estimation of Pore Connectivity and Permeability in Deepwater Carbonates with Construction of Multilayer Static and Dynamic Petrophysical Models. Presented at the SPWLA 53rd Annual Logging Symposium, Cartagena, Colombia, 16-20 June.

Donaldson, E.C. and Bizerra, M.J. 1985. Relationship of Wettability to Saturation Exponent. Presented at the 3rd International UNITAR/UNDP Heavy Crude and Tar Sands Conference.

Donaldson, E. C. and Siddiqui, T. K. 1989. Relation Between Archie Saturation Exponent and Wettability. *SPE Formation Evaluation* **4** (3): 359-362.

Dong, H. 2007. *Micro-CT Imaging and Pore Network Extraction*. PhD dissertation, Imperial College London, London, United Kingdom.

Doveton, J. H. 1994. Geological Log Interpretation: Reading the Rocks from Wire-Line Logs. SEPM Short Course 29, p.169.

Duda, A., Koza, Z., and Matyka, M. 2011. Hydraulic Tortuosity in Arbitrary Porous Media Flow. *Physical Review E* **84** (3). 036319.

Dullien, F. A. L. 1975. Prediction of "Tortuosity Tactors" from Pore Structure Data. *AICHE Journal* **21** (4): 820-822.

Dullien, F. A. L. 1979. *Porous Media: Fluid Transport and Pore Structure*. Academic Press.

Faris, S.R., Gournay, L.S., Lipson, L.B., and Webb, T.S. 1954. Verification of Tortuosity Equations. *Bulletin of the American Association of Petroleum Geologists*. **38**: 2226-2232.

Gandhi, A., Torres-Verdín, C., Voss, B., Gabulle, J., and Seminario F. 2010. Construction of Reliable Static and Dynamic Multi-Layer Petrophysical Models in Camisea Gas Reservoirs, Peru. SPWLA 51st Annual Logging Symposium, Perth, Australia, 19 - 23 June.

Gao, Y., Zhang, X., Rama, P., Liu, Y., Chen, R., Ostadi, H., and Jiang, K. 2012. Calculating the Anisotropic Permeability of Porous Media Using the Lattice Boltzmann Method and X-ray Computed Tomography. *Transport in Porous Media* **92** (2): 457-462.

Gao, X., Diniz da Costa J.C., and Bhatia S.K. 2014. Understanding the Diffusional Tortuosity of Porous Materials: An Effective Medium Theory Perspective. *Chemical Engineering Science* **110** (5): 55-71.

Garing C., Luquot L., Pezard P., and Gouze P. 2014. Electrical and Flow Properties of Highly Heterogeneous Carbonate Rocks. *Bulletin of the American Association of Petroleum Geologists* **1** (98): 49-66.

Garrouch, A.A., Ali, L., Qasem, F., and Ebrahim, A.S. 2001. Using Diffusion and Electrical Measurements to Assess Tortuosity of Porousmedia. *Industrial and Engineering Chemistry Research* **40**: 4363-4369.

Ghassemi, A. and Park, A. 2010. Pore Scale Study of Permeability and Tortuosity for Flow Through Particulate Media Using Lattice Boltzmann Method. *International Journal for Numerical and Analytical Methods in Geomechanics* **35** (8): 886-901.

Gommes, C.J., Bons, A.-J., Blacher, S., Dunsmuir, J.H., and Tsou, A.H. 2009. Practical Methods for Measuring the Tortuosity of Porous Materials from Binary or Gray-Tone Tomographic Reconstructions. *AIChE J.* **55** (8): 2000-2012.

Greenkorn, R.A. and Kessler, D.P. 1970. Dispersion In Heterogeneous Nonuniform Anisotropic Porous Media. *Industrial & Engineering Chemistry* **61** (9): 14-32.

Greenkorn, R.A. 1983. Flow Phenomena in Porous Media. *AIChE Journal.* **30** (1): 172-173.

Hamada, G. 2008. Accuracy Analysis of Water Saturation Models in Clean and Shaly Layers. Presented at the 2008 SPE Saudi Arabia Section Technical Symposium, Alkhobar, Saudi Arabia, 10-12 May.

Hossin, A. 1960. Calcul des Saturations En Eau Par la Methode du Ciment Argileux (formule d' Archie Generalisee). *Bulletin AFTP*: 125-128.

Hrabe, J., Hrabetova, S., and Segeth, K. 2004. A Model of Effective Diffusion and Tortuosity in the Extracellular Space of the Brain. *Biophysical Journal* **87**: 1606-1617.

Husten, P. and Anton, H. 1981. The Porosity Surface Concept Applied to Water Saturation Equations. Presented at the 7th European Formation Evaluation Symposium Transactions, Paris, France.

Iversen, N. and Jorgensen, B. 1993. Diffusion Coefficients of Sulfate and Methane in Marine Sediments: Influence of Porosity. *Geochimica et Cosmochimica Acta* **57** (3): 571-578.

Jing, X.D. 1990. *The Effect of Clay, Pressure and Temperature on the Electrical and Hydraulic Properties of Real and Synthetic Rocks*. PhD dissertation, Imperial College, London.

Juhasz, I. 1981. Normalised Qv - The Key To Shaly Sand Evaluation Using The Waxman-Smits Equation In The Absence Of Core Data. Presented at the 22nd SPWLA Annual Logging Symposium, Mexico City, Mexico, 23-26 June.

Karato, S. and Wang, D. 2012. Electrical Conductivity of Minerals and Rocks. *Physics and Chemistry of the Deep Earth.*

Katsube, T.J. 2010. *Review of Formation Resistivity Factor Equations Related to New Pore Structure Concepts*. Geological Survey of Canada.

Keller, G.V. 1953. Effect of Wettability on the Electrical Resistivity of Sand. *Oil and Gas J.* **51** (34): 62-65.

Khan, F., Enzmann, F., Kersten, M., Wiegmann, A., and Steiner, K. 2012. 3D Simulation of the Permeability Tensor in a Soil Aggregate on Basis of Nanotomographic Imaging and LBE Solver. *J. Soil Sediment* **12** (1): 86-96.

Kim, J., Ochoa, J., and Whitaker, S. 1987. Diffusion in Anisotropic Porous Media. *Transport in Porous Media* **2** (4): 327-356.

Knackstedt, M., Harris, R., Beck, G., Ghous, A., and Bauget, F. 2005. Resistivity Anisotropy Measured in Laminated Sands via Digital Core Analysis. Presented at the SPWLA 46th Annual Logging Symposium, New Orleans, Louisiana, USA, 26-29 June.

Kreamer, D., Weeks, E., and Thompson, G. 1988. A Field Technique to Measure the Tortuosity and Sorption-Affected Porosity for Gaseous Diffusion of Materials in the Unsaturated Zone with Experimental Results from Near Barnwell, South Carolina. *Water Resources Research* **24** (3): 331-341.

Latour, L., Klienberg, R., Mitra, P., and Sotak, C. 1993. Time-Dependent Diffusion Coefficient of Fluids in Porous Media as a Probe of Surface-to-Volume Ratio. *Journal of Magnetic Resonance, Series A* **101** (3): 342-346.

Latour, L., Klienberg, R., Mitra, P., and Sotak, C. 1995. Pore-Size Distributions and Tortuosity in Heterogeneous Porous Media. *Journal of Magnetic Resonance, Series A* **112** (1): 83-91.

Lewis, M. G. 1988. *The Effects of Stress and Wettability on Electrical Properties of Rocks*. MS thesis, University of Texas at Austin, Austin, Texas, USA.

Man, H. and Jing, X. 1999. Pore Network Modelling of Electrical Resistivity and Capillary Pressure Characteristics. *Transport in Porous Media* **41** (3): 263-285.

Mast, R. and Potter, P. 1963. Sedimentary Structures, Sand Shape Fabrics, and Permeability. II. *The Journal of Geology* **71** (5): 548-565.

Mauret, E. and Renaud, E. 1997. Transport Phenomena in Multi-Particle Systems—I. Limits of Applicability of Capillary Model in High Voidage Beds-Application to Fixed Beds of Fibers and Fluidized Beds of Spheres. *Chemical Engineering Science* **52** (11): 1807-1817.

Moore, C.H. 2001. Carbonate Reservoirs: Porosity Evolution and Diagenesis in a Sequence-Stratigraphic Framework. *Developments in Sedimentology* **19**: 155-163.

Morgan,W.B. and Pirson, S. J. 1964. The Effect of Fractional Wettability on the Archie Saturation Exponent. Presented at the 5th Annual logging symposium, Midland, Texas, USA, 13-15 May.

Moss, A.K., Jing, X.D., and Archer, J.S. 1999. Laboratory Investigation of Wettability and Hysteresis Effects on Resistivity Index and Capillary Pressure Characteristics. *Journal of Petroleum Science and Engineering* **24** (2): 231-242.

Mota, M., Teixeira, J.A., Bowen, R., and Yelshin, A. 2001. Binary Spherical Particle Mixed Beds: Porosity and Permeability Relationship Measurement. *The Filtration Society* **1** (4): 101-106.

Mukerji, T. and Mavko, G., 1994. Scale-Dependent Dynamic Wave Propagation in Heterogeneous Media: II. Theory. Presented at the SEG Annual Meeting, Los Angeles, California, USA, 23-28 October.

Mungan, N. and Moore, E. J. 1968. Certain Wettability Effects on Electrical Resistivity in Porous Media. *J. Can. Petr. Tech.* **7** (1): 20-25.

Nakashima, Y. Nakano, T. Nakamura, K. Uesugi, K. Tsuchiyama, A. and Ikeda S. 2004. Three-dimensional Diffusion of Non-sorbing Species in Porous Sandstone: Computer Simulation Based on X-ray Microtomography using Synchrotron Radiation. *Journal of Contaminant Hydrology* **74** (1): 253-264.

Nakashima, Y. and Kamiya, S. 2007. Mathematica Programs for the Analysis of Three-Dimensional Pore Connectivity and Anisotropic Tortuosity of Porous Rocks using X-ray Computed Tomography Image Data. *Journal of Nuclear Science and Technology* **44** (9): 1233-1247.

Ohkubo, T. 2008. Tortuosity Based on Anisotropic Diffusion Process in Structured Plate-like Obstacles by Monte Carlo Simulation. *Transport in Porous Media* **72** (3): 339-350.

Patchett, J. G. and Herrick, D. C. 1982. A Review of Saturation Models. In: Shaly Sand Reprint Volume. SPWLA.

Patchett, J. G. and Rausch, R. W. 1967. An Approach to Determining Water Saturation in Shaly Sands. *SPE J.* **19** (10): 1395-1406.

Pfleiderer, S. and Halls, H. C. 1990. Magnetic Susceptibility Anisotropy of Rocks Saturated with Ferrofluid: A New Method to Study Pore Fabric? *Physics of the Earth and Planetary Interiors*. **65** (1-2): 158-164.

Pirson, S.J. 1983. *Geologic Well Log Analysis*. Houston, TX: Gulf Publishing.

Pittman, E.D. 1992. Relationship of Porosity and Permeability to Various Parameters Derived from Mercury Injection-Capillary Pressure Curves for Sandstone. *AAPG Bulletin* **76** (2): 191 -198.

Poupon, A., Loy, M.E., and Tixier, M.F. 1954. A Contribution to Electric Log Interpretation in Shaly Sands. In *AIME Transactions*.

Poupon, A., and Leveaux, J. 1971. Evaluation of Water Saturations in Shaly Formations. Presented at the SPWLA 12th Annual Logging Symposium, Dallas, Texas, 2-5 May.

Ransom, P.C. 1984. A Contribution Toward a Better Understanding of The Modified Archie Formation Resistivity Factor Relationship. *Petrophysicists* **25** (2): (7-12).

Rice, P., Fontugne, D., Latini, R., and Barduhn, A. 1970. Anisotropic Permeability in Porous Media. *Industrial & Engineering Chemistry* **62** (6): 23-31.

Rust, C. F. 1957. A Laboratory Study of Wettability Effects on Electrical Resistivity in Porous Media. Presented at the SPE Venezuelan Second Annual Meeting, Caracas, Venezuela, 6-9 November.

Salazar, J.M., 2004, *Assessment of Permeability from Well Logs on Core Calibration and Simulation of Mud-Filtrate Invasion*. MS thesis, The University of Texas at Austin, Austin, Texas.

Salem, H. and Chiligarian, G. 2000. Influence of Porosity and Direction of Flow on Tortuosity in Unconsolidated Porous Media. *Energy Sources* **22** (3): 207-213.

Scheidegger, and Adrian, E. 1954. Directional Permeability of Porous Media to Homogeneous Fluids. *Pure and Applied Geophysics* **28** (1): 75-90.

Schlumberger. 1972. Log interpretation, Vol. I: Principles. New York, Schlumberger Limited, p.113.

Schlumberger. 1974. Log interpretation, Vol. II: Applications. New York, Schlumberger Limited, p.116.

Schneider, C.A., Rasband, W.S., and Eliceiri, K.W. 2012. NIH Image to ImageJ: 25 Years of Image Analysis. *Nature Methods* **9** (7): 671-675.

Selomulya, C., Tran, T., and Jia, X. 2006. An Integrated Methodology to Evaluate Permeability from Measured Microstructures. *AICHE Journal* **52** (10): 3394-3400.

Sen, P. 2004. Time-Dependent Diffusion Coefficient as a Probe of Geometry. *Concepts in Magnetic Resonance Part A* **23A** (1): 1-24.

Serra, O. and Abbott, H.T., 1980. The Contribution of Logging Data to Sedimentology and Stratigraphy. Presented at 55th SPE Annual Fall Technical Conference and Exhibition, Dallas, Texas. SPE-9270.

Sherwood, C.N. and Satterfield, T.K. 1963. *Role of Diffusion in Catalysis.* Addison-Wesley.

Siegesmund, S., Kern, H., and Vollbrecht, A. 1991. The Effect of Oriented Microcracks on Seismic Velocities in an Ultramylonite. *Tectonophysics* **186** (3-4): 241-251.

Simandoux, P. 1963. Dielectric Measurements on Porous Media: Application to the Measurement of Water Saturations: Study of the Behaviour of Argillaceous Formations. *Reveu De l'Institute Francais du Petrole* **18**: 193-215.

Suman, R. and Knight, R. 1997. Effects of Pore Structure and Wettability on the Electrical Resistivity of Partially Saturated Rocks—A Network Study. *Geophysics* **62** (4): 1151-1162.

Swanson, B. F. 1985. Microporosity in Reservoir Rocks - its Measurement and Influence on Electrical Resistivity. Paper Presented at the SPWLA 26th Annual Logging Symposium, Dallas, Texas, USA, 17-20 June.

Sweeney, S.A. and Jennings, H.V. 1960. The Electrical Resistivity of Preferentially Water-Wet and Preferentially Oil-Wet Carbonate Rocks. *Producers Monthly* **24** (7): 29-32.

Teh, W.J., Willhite, G.P., Doveton, J. H., and Tsau, J.S. 2011. Pore Morphology Effect in Microlog for Porosity Prediction in a Mature Field: Presented at the SPE Eastern Regional Meeting, Columbus, Ohio, USA, 17-19 August.

Theys, P.P. 1999. *Log Data Acquisition and Quality Control*. 2nd Edition, Technip.

Tsakiroglou, C. D., and Payatakes, A. C. 1991. Effects of Pore-Size Correlations on Mercury Porosimetry Curves. *J. Colloid and Interface Science* **146** (2): 479-494.

Verwer, K., Eberli, G.P., and Weger R.J. 2011. Effects of Pore Structure on Electrical Resistivity in Carbonates. *AAPG Bulletin*, **95** (2): 175-190.

Wardlaw, N. C., Li, Y., and Forbes, D. 1987. Pore-Throat Size Correlations from Capillary Pressure Curves. *Transport in Porous Media* **2** (6): 597-614.

Waxman, M.H. and Smits, L.J., 1968. Electrical Conductivities in Oil-Bearing Shaly Sand. *SPE J.* **8** (2): 107-122.

Weissberg, H.L. 1963. Effective Diffusion Coefficients in Porous Media. *Journal of Applied Physics* **34** (1): 2636-2639.

Whitaker, S. 1999. *The Method of Volume Averaging*, First edition. Springer Science & Business Media.

Widarsono, B. 2012. Choice of Water Saturation Model in Log Analysis and its Implication to Water Saturation Estimates — a Further Investigation. *Scientific Contributions Oil & Gas* **35** (3): 99-107.

Winsauer, W.O., Shearin, H.M., Masson, P.H., and William, M. 1952. Resistivity of Brine-Saturated Sands in Relation to Pore Geometry. *Bulletin of the American Association of Petroleum Geologists* **36**: 253-277.

Witt, K. J. and Brauns, J. 1983. Permeability-Anisotropy Due to Particle Shape. *Journal of Geotechnical and Geoenvironmental Engineering* **109** (9): 1181-1187.

Woodhouse, R. 1976. Athabasca Tar Sand reservoir properties derived from cores and logs. Presented at the SPWLA 17th Annual Logging Symposium, Denver, Colorado, USA, 9-12 June.

Worthington, P. F. 1985. The Evolution of Shaly-Sand Concepts In Reservoir Evaluation. *Petrophysicists Journal* **26** (1): 23-40.

Worthington, P.F., Pallatt, N., and Toussaint-Jackson, J.E. 1989. Influence of Microporosity on The Evaluation of Hydrocarbon Saturation. *SPE Formation Evaluation* **4** (2): 203-209.

Worthington, P.F. and Pallatt, N. 1992. Effect of Variable Saturation Exponent on the Evaluation of Hydrocarbon Saturation. *SPE Formation Evaluation* **7** (4): 331-336.

Wyllie, M.R.J. and Spangler, M.B. 1952. Application of Electrical Resistivity Measurements to Problem of Fluid Flow in Porous Media. *AAPG Bulletin* **36**: 359-403.

Xu, C. 2013. *Reservoir Description with Well-Log-Based and Core-Calibrated Petrophysical Rock Classification*. PhD dissertation, University of Texas at Austin, Austin, Texas (August 2013).

Yin, H., Mavko, G., Mukerji, T., and Nur, A., 1994. Scale-Dependent Dynamic Wave Propagation In Heterogeneous Media: I. Experiments. Presented at the SEG Annual Meeting, Los Angeles, California, USA, 23-28 October.